Supporting Information

for

Shortwave infrared imaging with J-aggregates stabilized in hollow mesoporous silica nanoparticles

Wei Chen[#,†,‡], Chi-An Cheng[§,†,‡], Emily D. Cosco[#,⊥,‡], Shyam Ramakrishnan[⊥], Jakob G. P. Lingg[⊥], Oliver T. Bruns[⊥,*], Jeffrey I. Zink[#,†,*], and Ellen M. Sletten[#,†,*]

[#]*Department of Chemistry and Biochemistry,* [§]*Department of Bioengineering,* [†]*California NanoSystems Institute, University of California, Los Angeles, Los Angeles, California 90095, United States*

[⊥]*Helmholtz Pioneer Campus, Helmholtz Zentrum München, D-85764 Neuherberg, Germany*

*Oliver T. Bruns: oliver.bruns@helmholtz-muenchen.de

*Jeffrey I. Zink: zink@chem.ucla.edu

*Ellen M. Sletten: sletten@chem.ucla.edu

Table of Contents

I. Materials and general experimental procedures…… S4
Materials
Instrumentation
Abbreviations
Cell culture procedures
Animal procedures
SWIR imaging apparatus

II. Synthetic procedures ……... S6
Synthesis of Stöber silica spheres
Synthesis of hollow mesoporous silica nanoparticles (HMSNs)
Synthesis of APTS functionalized HMSNs (HMSNs-APTS)
Synthesis of APTS functionalized Stöber silica spheres
Loading of IR-140 in HMSNs, HMSNs-APTS, or $dSiO_2$@MSNs
PEG conjugation on the surface of IR-140 loaded HMSNs-APTS

III. Supporting schemes ……... S8
Scheme S1: Synthesis of hollow mesoporous silica nanoparticles (HMSNs)
Scheme S2: Synthesis of IR-140-loaded HMSN-PEG

IV. Supporting figures …… S10
Figure S1: TEM images of Stöber silica spheres, $dSiO_2$@MSNs, and HMSNs
Figure S2: UV/Vis/NIR spectra of IR-140 loaded HMSNs or $dSiO_2$@MSNs for washing optimization
Figure S3: UV/Vis/NIR spectra and zeta potential of Stöber silica spheres and Stöber silica spheres-APTS
Figure S4: Nitrogen adsorption/desorption isotherms and pore diameter distributions of HMSNs, HMSNs-APTS, and $dSiO_2$@MSNs
Figure S5: UV/Vis/NIR spectra of IR-140 loaded HMSNs, Stöber silica spheres, Stöber silica spheres-APTS, or $dSiO_2$@MSNs
Figure S6: Loading capacity of IR-140 in HMSNs and HMSNs-APTS
Figure S7: TEM images of HMSNs with and without IR-140 treatment
Figure S8: UV/Vis/NIR spectra of IR-140 HMSNs-APTS for loading optimization
Figure S9: DLS size distribution of HMSNs-PEG and synthetic intermediates
Figure S10: Zeta potential of HMSNs-PEG and synthetic intermediates
Figure S11: UV/Vis/NIR characterization of IR-140 J-aggregate formation in solution
Figure S12: Emission of monomer and J-aggregate states of IR-140 under 980 nm excitation
Figure S13: Stability of J-aggregates over time
Figure S14: Photostability of J-aggregates in the presence and absence of oxygen
Figure S15: Cytotoxicity study of IR-140 loaded HMSNs-PEG examined by a CCK-8 assay
Figure S16: *In vivo* images of IR-140 HMSNs-PEG delivery over one hour

V. Figure and supporting figure experimental procedures ……... S24

VI. Supporting tables ……..... S31
Table S1: Photophysical characterization
Table S2: Photobleaching rates

VII. Supplementary notes ……... S32

Note S1: Estimation of the amount of dye molecules in a single HMSN and HMSN-PEG
Note S2: Absorption coefficients
Note S3: Quantum yield
Note S4: Photobleaching rates
Figure S17: Cartoon figure of HMSN or HMSN-APTS used in this work
Figure S18: Absorption coefficient of IR-140 monomer in DMSO
Figure S19: Uncorrected absorption coefficient of IR-140 J-aggregate in 35% DMSO/0.9% NaCl in water
Figure S20: Corrected absorption coefficient of IR-140 J-aggregate in 35% DMSO/0.9% NaCl in water
Figure S21: Solvent corrected integrated fluorescence intensity versus absorbance plots
Figure S22: Photobleaching data plotted as the ln[A] vs time and the corresponding linear fits
Table S3: Photobleaching rates and values used in calculations and corrections

VIII. References …… S40

I. Materials and general experimental procedures

Materials

IR-140 (95%), cetyltrimethylammonium chloride (CTAC, 25 wt% in water), cetyltrimethylammonium bromide (CTAB, 99+%), tetraethyl orthosilicate (TEOS, 98%), (3-aminopropyl)triethoxysilane (APTS, 99%), ammonium nitrate (NH_4NO_3, 98+%), triethanolamine (TEA, 99+%), 2-(*N*-morpholino)ethanesulfonic acid hydrate (MES hydrate, 99.5+%), and phosphate buffer saline (X10) were purchased from Sigma-Aldrich. Sodium carbonate anhydrous (99.5+%) was purchased from EMD Millipore. Alpha-methoxy-omega-carboxylic acid poly(ethylene glycol) (MeO-PEG-COOH, Mw = 23,000 Da) was purchased from Iris Biotech GmbH. Ethanol (200 proof) was purchased from Decon Laboratories, Inc. 1-Ethyl-3-(-3-dimethylaminopropyl) carbodiimide hydrochloride (EDC-HCl, 99+%), and *N*-hydroxysulfosuccinimide sodium salt (sulfo-NHS, 99+%) were purchased from CovaChem. Dimethyl sulfoxide (DMSO, 99.9+%), sodium hydroxide (NaOH, 97+%), and ammonium hydroxide (NH_4OH) purchased from Fisher Scientific. Dulbecco's modified Eagle's medium (DMEM) with high glucose, fetal bovine serum (FBS), antibiotics (10,000 U/mL penicillin, 10,000 μg/mL streptomycin, and 29.2 mg/mL L-glutamine), trypsin-ethylenediaminetetraacetic acid (trypsin-EDTA) (0.05 %), and Dulbecco's phosphate-buffered saline (DPBS) were purchased from Gibco. Cell counting kit-8 (CCK-8) was purchased from Dojindo Molecular Technologies, Inc. All chemicals were used without further purification.

Instrumentation

Bath sonication was performed using a Branson 3800 ultrasonic cleaner or an Elma S15 Elmasonic. Masses for analytical measurements were taken on a Sartorius MSE6.6S-000-DM or MSA6.6S-000-DM Cubis Micro Balance. Absorbance spectra were collected on a JASCO V-770 UV/Vis/NIR spectrophotometer with a 2000 nm/min scan rate after blanking with the appropriate solvent, on a Cary 5000 UV-Vis-NIR spectrophotometer or on a Shimadzu UV-1800 UV-Visible Scanning Spectrophotometer. Photoluminescence spectra were obtained on a Horiba Instruments PTI QuantaMaster Series fluorometer. Quartz cuvettes (10 mm, 3 mm and 2 mm) were used for absorbance and photoluminescence measurements. The dynamic light scattering (DLS) measurements were performed on a ZETAPALS instrument with a 660 nm red diode laser (Brookhaven Instruments Corporation). Zeta potential value was measured on a Malvern Zetasizer Nano at room temperature. Nitrogen adsorption/desorption isotherms were acquired at 77 K on a Autosorb-iQ, Quantachrome Instruments. Transmission electron microscopy was performed on a Tecnai T12 instrument with an operating voltage of 120 kV. Animal imaging was performed on custom instrumentation described below.

Abbreviations

(3-Aminopropyl)triethoxysilane (APTS), Brunauer-Emmett-Teller (BET), Barrett-Joyner-Halenda (BJH), Cell counting kit-8 (CCK-8), Cetyltrimethylammonium bromide (CTAB), Cetyltrimethylammonium chloride (CTAC), Dichloroethane (DCE), Dichloromethane (DCM), dynamic light scattering (DLS), Dulbecco's modified Eagle's medium (DMEM), Dimethylsulfoxide (DMSO), Dulbecco's phosphate-buffered saline (DPBS), 1-Ethyl-3-(-3-dimethylaminopropyl) carbodiimide hydrochloride (EDC-HCl), Fetal bovine serum (FBS), frames per second (fps), hollow mesoporous silica nanoparticles (HMSNs), PEGylated HMSNs (HMSNs-PEG), Alpha-methoxy-omega-carboxylic acid poly(ethylene glycol) (MeO-PEG-COOH), 2-(*N*-

morpholino)ethanesulfonic acid (MES), Sodium Chloride (NaCl), Sodium hydroxide (NaOH), Ammonium nitrate (NH_4NO_3), Ammonium hydroxide (NH_4OH), Near-infrared (NIR), Phosphate buffer saline (PBS), Poly(ethylene glycol) (PEG), *N*-hydroxysulfosuccinimide sodium salt (sulfo-NHS), Shortwave infrared (SWIR), Triethanolamine (TEA), transmission electron microscope (TEM), Tetraethyl orthosilicate (TEOS), Trypsin-ethylenediaminetetraacetic acid (trypsin-EDTA)

Cell culture procedures

HeLa cells, a cervical cancer cells line, were cultured in T-75 flasks (Corning) with vented caps in a high glucose Dulbecco's modified Eagle's medium (DMEM) supplemented with 10 % fetal bovine serum (FBS), and 1 % antibiotics (100 U/mL penicillin and 100 µg/mL streptomycin) in a humidity-controlled incubator at 37 °C with 5% CO_2. The HeLa culture media were daily changed and the cells were harvested by trypsinization with 0.05% trypsin-ethylenediaminetetraacetic acid (EDTA) for passaging every 2–3 days.

Animal procedures

Animal experiments were conducted in accordance with the approved institutional protocols of Helmholtz Zentrum München. Non-invasive whole mouse imaging was performed on two six-week old female CD-1 nude mice (22.4 g, 19.1 g), purchased from Charles River Laboratories. Mice were anesthetized with an i.p. injection of a ketamine/xylazine mixture. Tail vein injections were performed with a catheter assembled from a 30 ga needle connected through plastic tubing to a second 30 ga needle with syringe prefilled with isotonic saline solution. The bevel of the needle was then inserted into the tail vein and secured using tissue adhesive.

SWIR imaging apparatus

For whole mouse imaging, we used a custom-built setup. A 35 W 980 nm laser (Lumics LU0980D350-D30AN) was coupled in a fiber (600 µm core, Thorlabs BF46LS01) The output from the fiber was fixed in an excitation cube and reflected off of a mirror (Thorlabs BBE1-E03), and passed through a positive achromat (Thorlabs AC254-050-B), 1000 nm shortpass filter (Thorlabs FESH 1000), and an engineered diffuser (Thorlabs ED1-S20-MD) to provide uniform illumination over the working area. The excitation flux at the object was adjusted to be close to 100 $mWcm^{-2}$ with an error of ± 3% (power density used is defined separately in each experiment). The working area was covered by a heating mat coated with blackout fabric (Thorlabs BK5). A 4-inch square first-surface silver mirror (Edmund Optics, 84448) was used to direct the emitted light through a custom filter set (Thorlabs NF980-41, 3x FELH1000, 2x FGL1000) to an Allied Vision Goldeye G-032 Cool TEC2 camera with sensor set point at -30 °C, equipped with a C-mount camera lens (Navitar, SWIR-35). The assembly was partially enclosed to avoid excess light while enabling manipulation of the field of view during operation. The image acquisition toolbox of MATLAB programming environment is used in combination with a custom MATLAB script to preview and collect the required image data. The prepared MATLAB script allows users to access basic functionalities of the image acquisition device by establishing a packet jitter free data streaming link between the desktop computer and the acquisition device.

II. Synthetic Procedures

Synthesis of Stöber silica spheres

Stöber silica spheres were synthesized by a sol-gel reaction in basic solution as reported previously.[1] Briefly, NH_4OH (1.6 mL) was dissolved in a mixture of ethanol (71.4 mL) and D.I. water (10 mL) in a 250 mL flask with vigorous stirring. After stirring for 10 min at room temperature, TEOS (2 mL) was rapidly added to the solution which was further stirred for 1 h at room temperature for the formation of Stöber silica nanoparticles. Afterwards, the solution containing Stöber silica spheres was centrifuged (7830 rpm, 7197 g, 20 min) and washed with ethanol and D.I. water twice, respectively. The Stöber silica spheres were finally dispersed in 40 mL of D.I. water for further use.

Synthesis of hollow mesoporous silica nanoparticles (HMSNs)

The synthesis of hollow mesoporous silica nanoparticles (HMSNs) was carried out by using Stöber silica spheres as the hard templates which were later removed by selective etching in a basic solution. First, CTAC (2 g, 25 wt% in water solution) and TEA (20 mg) were dissolved in D.I. water (20 mL) in a 100 mL round-bottom flask with vigorous stirring at 80 °C. The reaction mixture was stirred for 5 min followed by the addition of 10 mL of Stöber silica sphere solution prepared as described above, and stirred for 20 min. To coat mesoporous silica on the surface of Stöber silica spheres, TEOS (150 µL) was added dropwise to the solution with vigorous stirring. The nanoparticles were designated as $dSiO_2$@MSNs (Scheme S1). After 1 h, the solution was cooled to 50 °C and sodium carbonate (1.89 g) dissolved in D.I. water (3 mL) was added to selectively etch the Stöber silica sphere template in the mesoporous silica shell. The etching process was carried out at 50 °C for 2 h. Afterwards, the solution containing HMSNs were centrifuged (7830 rpm, 7197 g, 15 min) and washed with ethanol 3 times (3 x 50 mL) to remove the unreacted impurities. To remove the CTAC surfactant templates, HMSNs were dispersed in 50 mL of ethanol containing NH_4NO_3 (1 g). The solution was brought to 60 °C with vigorous stirring. After 1 h, the solution was cooled to room temperature, centrifuged (7830 rpm, 7197 g, 15 min), and washed once with ethanol (50 mL). The surfactant removal process was repeated two more times. Finally, surfactant free HMSNs were washed with D.I. water (2 x 50 mL) and ethanol (2 x 50 mL), respectively and stored in 10 mL of absolute ethanol for further use.

Synthesis of APTS functionalized HMSNs (HMSNs-APTS)

APTS functionalized HMSNs (HMSNs-APTS) were synthesized by procedures similar to those of HMSNs. First, CTAC (2 g, 25 wt% in water solution) and TEA (20 mg) were dissolved in D.I. water (20 mL) in a 100 mL round-bottom flask with vigorous stirring at 80 °C. The reaction solution was stirred for 5 min followed by the addition of 10 mL of Stöber silica sphere solution prepared as described above. After stirring for 20 min, TEOS (150 µL) was added dropwise to the solution with vigorous stirring. After 1 h, a mixture of APTS (40 µL) and ethanol (120 µL) was added to the solution followed by stirring for another 1 h at 80 °C to conjugate APTS on the surface of HMSNs. The Stöber silica sphere etching and surfactant removal processes were the same as described in the synthesis of HMSNs section. The resulting nanoparticles were dispersed in ethanol and designated as HMSNs-APTS.

Synthesis of APTS functionalized Stöber silica Spheres

The Stöber silica spheres (80 mg) were dispersed in a mixture of ethanol (20 mL) and APTS (10 μL). The solution was stirred at room temperature for 5 min and was brought to 78 °C. Then, the solution was refluxed for 12 h with vigorous stirring. Subsequently, the solution was cooled to room temperature, and APTS functionalized Stöber silica spheres (Stöber silica spheres-APTS) were washed twice (2 x 20 mL) with ethanol and stored in 10 mL of absolute ethanol for further use.

Loading of IR-140 in HMSNs, HMSNs-APTS, or $dSiO_2$@MSNs

HMSNs, HMSNs-APTS, or $dSiO_2$@MSNs (2 mg) dispersed in ethanol were centrifuged (14000 rpm, 16873 g, 15 min) and washed with DMSO (3 x 1 mL) before IR-140 loading. HMSNs or HMSNs-APTS were then dispersed in 200 μL of a DMSO solution containing 5, 10, or 20 mM IR-140 by sonication in a bath sonicator for 10 min. For $dSiO_2$@MSNs, the nanoparticles were dispersed in 200 μL of a DMSO solution containing 5, or 20 mM IR-140 by sonication in a bath sonicator for 10 min. After stirring the solution for 20 h to make IR-140 diffuse into the pores and cavity of HMSNs, HMSNs-APTS, or $dSiO_2$@MSNs, the solution containing the particles was centrifuged (14000 rpm, 16873 g, 15 min) and the supernatant was kept for loading capacity calculations. Then, IR-140 loaded HMSNs were washed with three different methods: (a) washed with PBS (1 mL) using a water bath sonication, (b) gently washed with PBS (1 mL) by using plastic transfer pipettes, and (c) washed with water (1 mL) by using plastic transfer pipettes, respectively, to remove free DMSO and DMSO loaded in the pores. IR-140 loaded HMSNs-APTS, or IR-140 loaded $dSiO_2$@MSNs were washed only by method (b). Afterwards, IR-140 loaded nanoparticles were centrifuged (8000 rpm, 5510 g, 3 min) to remove the supernatant. The washing steps were repeated 5 times. Finally, IR-140 loaded HMSNs, HMSNs-APTS, or $dSiO_2$@MSNs were re-dispersed in PBS (1 mL) solution by sonication.

PEG conjugation on the surface of IR-140 loaded HMSNs-APTS (HMSNs-PEG preparation)

To increase the colloidal stability, PEG was conjugated on the surface of IR-140 loaded HMSNs-APTS via amide bond formation. After IR-140 was loaded in HMSNs-APTS, the nanoparticles were gently washed with PBS (5 x 1 mL), D.I. water (2 x 1 mL), and MES buffer solution (pH = 6.0, 10 mM) (1 x 1 mL), respectively. Finally, IR-140 loaded HMSNs-APTS (2 mg) were dispersed in MES buffer (1 mL) by sonication. Alpha-methoxy-omega-carboxylic acid poly(ethylene glycol) (MeO-PEG-COOH, CAS No. 92450-99-2) (10 mg) was dissolved in MES buffer (200 μL) followed by the addition of EDC-HCl (5 mg) and sulfo-NHS (2.5 mg) pre-dissolved in MES buffer (300 μL). The solution was stirred for 30 min. Then, the MES buffer solution containing the activated MeO-PEG-COOH (500 μL) was added to 1 mL of 2 mg/mL IR-140 loaded HMSNs-APTS MES solution. The solution was further mixed and stirred for 20 h to conjugate PEG on the surface of IR-140 loaded HMSNs-APTS. Then, IR-140 loaded HMSNs-PEG were centrifuged (10000 rpm, 8609 g, 10 min) and washed with D.I. water (2 x 1 mL) and PBS (1 x 1 mL) to remove the excess MeO-PEG-COOH, EDC-HCl, sulfo-NHS, and MES buffer solution. Finally, IR-140 loaded HMSNs-PEG were dispersed in PBS buffer (1 mL) solution for UV/Vis/NIR or photoluminescence measurements.

III. Supporting schemes

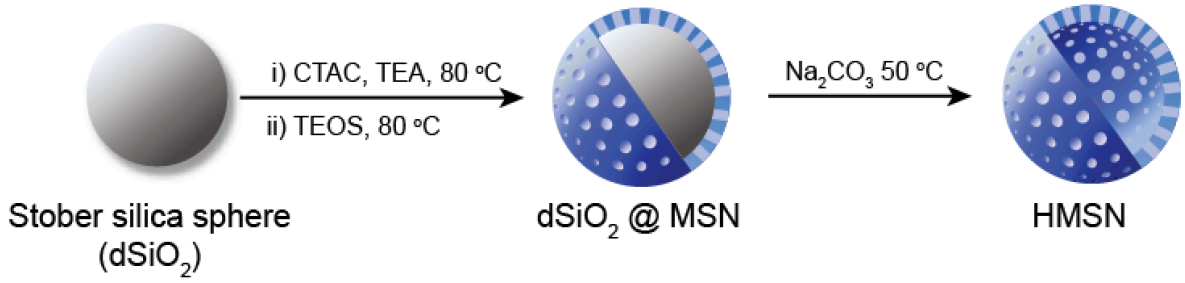

Scheme S1. Synthesis of hollow mesoporous silica nanoparticles (HMSNs).

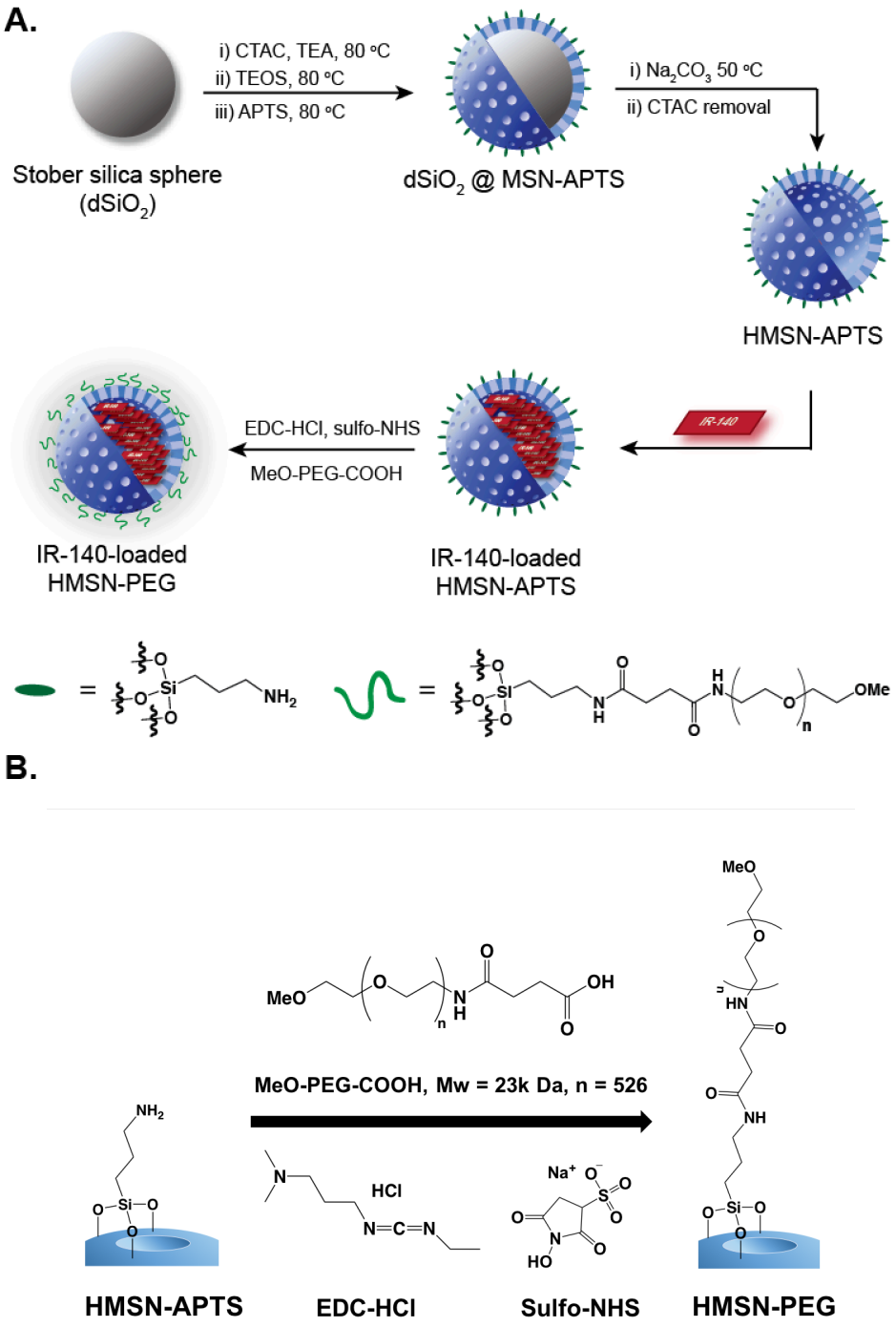

Scheme S2. Synthesis of IR-140-loaded HMSN-PEG. A) Overall synthesis starting from Stöber spheres. B) Detailed schematic of conjugation of PEG to the surface of HMSN-APTS. Note that we believe the APTS modification is only on the outer surface due to the Stöber silica sphere blocking the inner surface and the CTAC surfactant blocking the pores.[2-4]

IV. Supporting figures

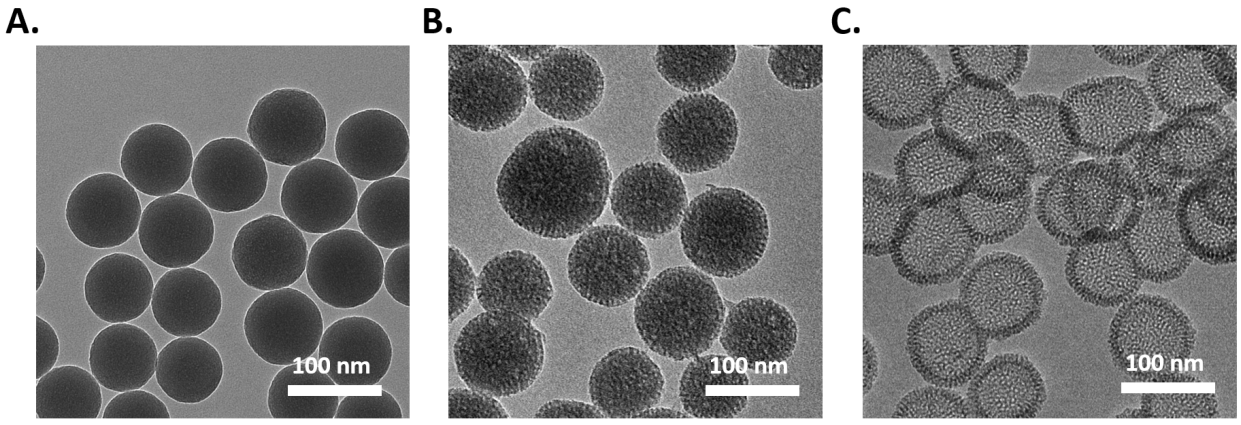

Figure S1. TEM images of (A) Stöber silica spheres, (B) $dSiO_2$@MSNs, and (C) HMSNs. The nanoparticles were dispersed in ethanol at a concentration of 0.1 mg/mL. TEM images were measured on a Tecnai T12 instrument with an operating voltage of 120 kV.

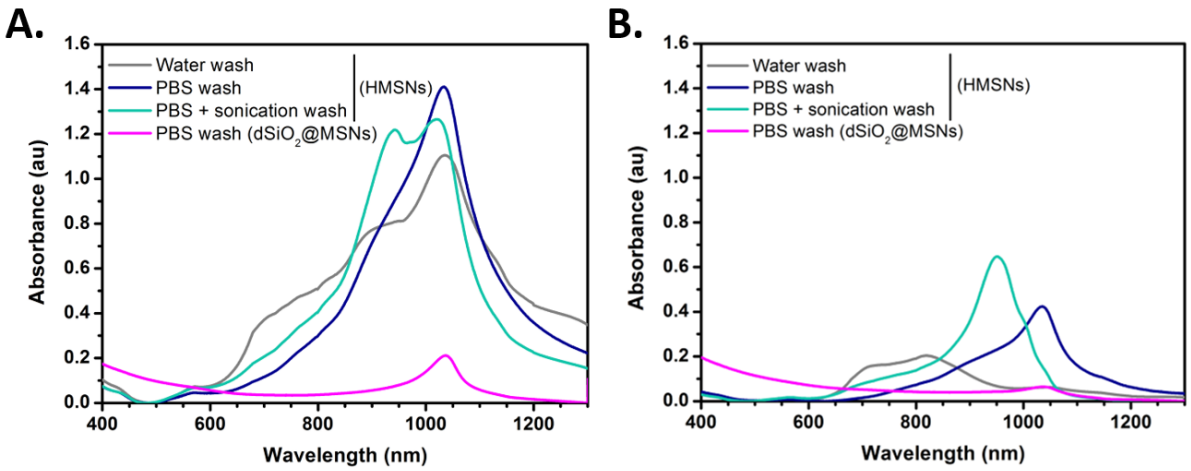

Figure S2. UV/Vis/NIR spectra of HMSNs or $dSiO_2$@MSNs containing IR-140. The loading concentrations of IR-140 were (A) 20 mM and (B) 5 mM; HMSNs or $dSiO_2$@MSNs were loaded at 10 mg/mL. The HMSNs particles were washed by methods (a, PBS with sonication, teal), (b, PBS, blue), or (c, water, gray) (5x, 1 mL), or the $dSiO_2$@MSNs were washed by method (b, PBS, magenta) (see Section II, synthetic procedures). The absorbance spectra were measured with 10 mm quartz cuvettes at 0.25 mg nanoparticles/mL in PBS.

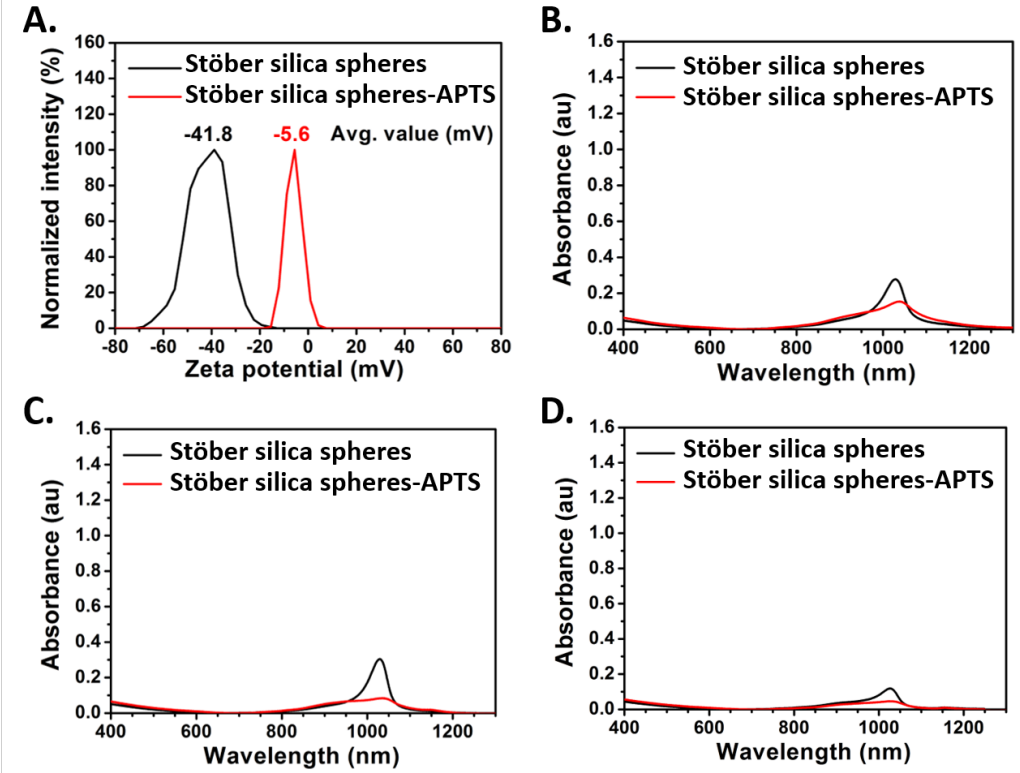

Figure S3. Control experiment with Stöber silica spheres. A) The zeta potential of Stöber silica spheres (black), and Stöber silica spheres-APTS (red) in D.I. water at 0.05 mg/mL at room temperature. In the case of the APTS-modified Stöber spheres, we believe the surface is saturated with APTS as higher concentrations of APTS did not significantly change the zeta potential. B/C/D) UV/Vis/NIR spectra of Stöber silica spheres (black) or Stöber silica spheres-APTS (red) containing IR-140. The loading concentrations of IR-140 were (B) 20 mM, (C) 10 mM, or (D) 5 mM; Stöber silica spheres or Stöber silica spheres-APTS were loaded at 10 mg/mL. After the loading, the particles were washed with PBS (5x, 1 mL). The absorbance spectra were measured with 10 mm quartz cuvettes at 0.25 mg nanoparticles/mL PBS.

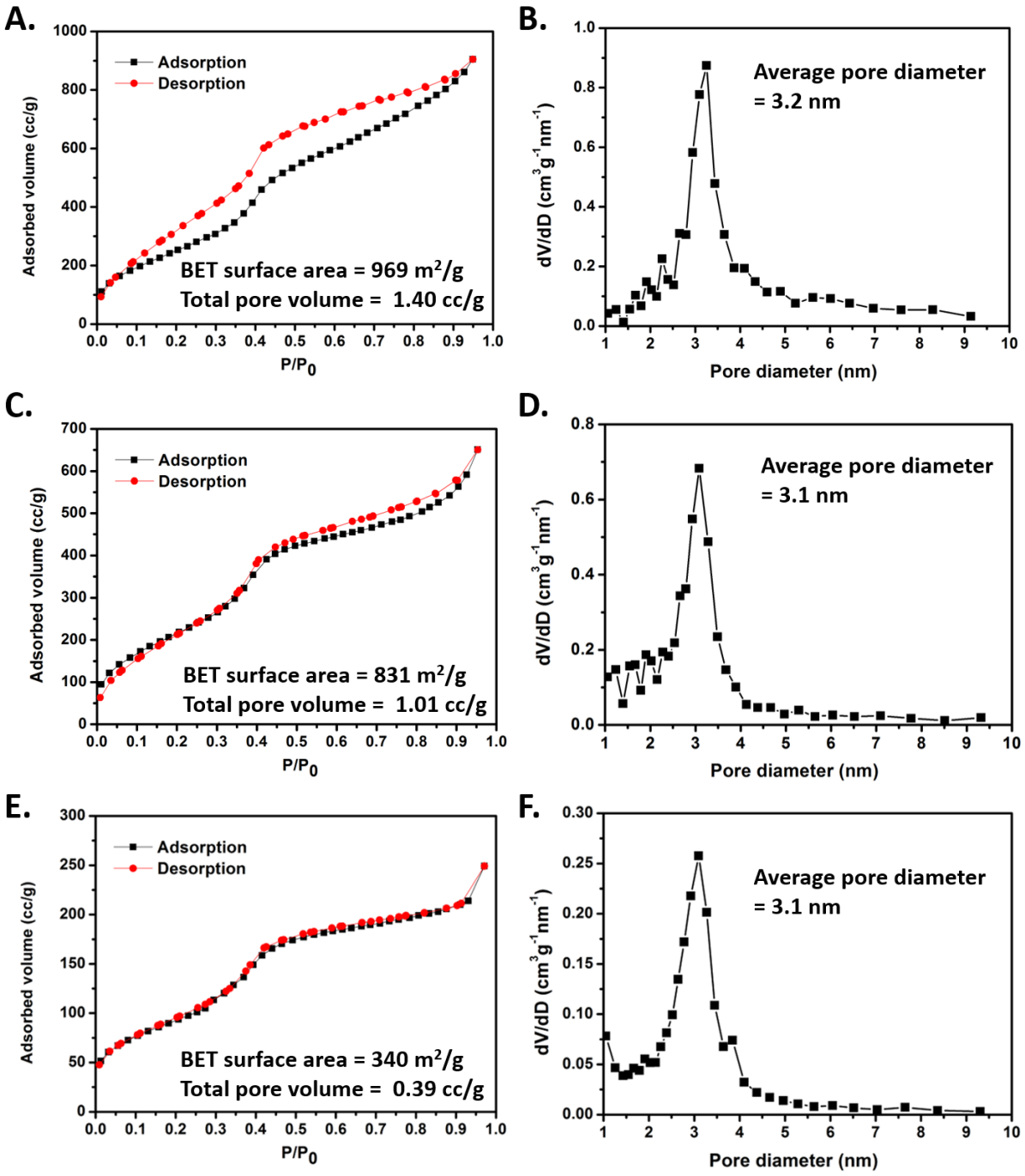

Figure S4. Nitrogen adsorption (black)/desorption (red) isotherms of (A) HMSNs, (C) HMSNs-APTS, and (E) $dSiO_2$@MSNs. The BET surface areas of HMSNs, HMSNs-APTS, and $dSiO_2$@MSNs are 969 m^2/g, 831 m^2/g, and 340 m^2/g, respectively. The total pore volumes of HMSNs, HMSNs-APTS, and $dSiO_2$@MSNs are 1.40 cc/g, 1.01 cc/g, and 0.39 cc/g, respectively. Pore diameter distributions of (B) HMSNs, (D) HMSNs-APTS, and (F) $dSiO_2$@MSNs. The average pore diameters are 3.2 nm, 3.1 nm, and 3.1 nm, respectively.

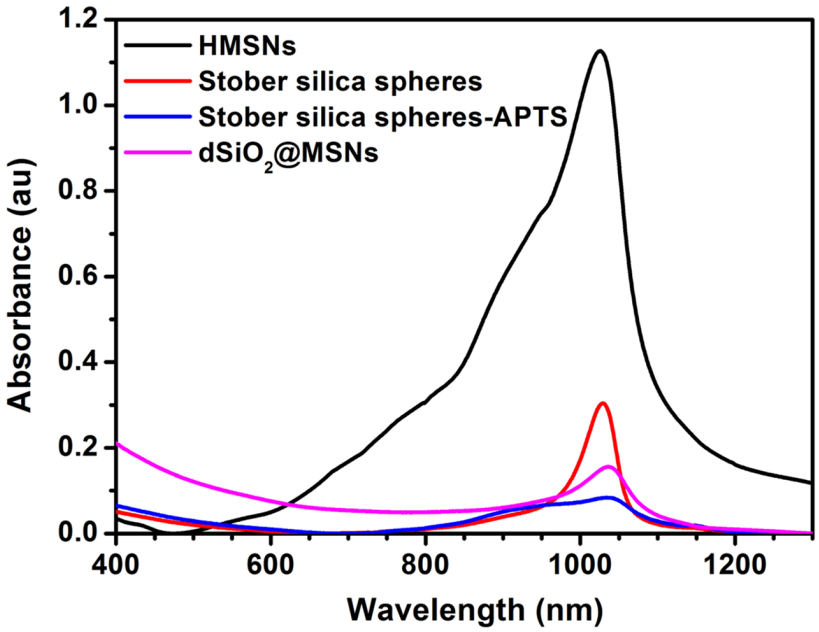

Figure S5. UV/Vis/NIR spectra of IR-140 loaded HMSNs, Stöber silica spheres, Stöber silica spheres-APTS, or $dSiO_2$@MSNs. The loading concentrations of IR-140 were 10 mM; HMSNs, Stöber silica spheres, Stöber silica spheres-APTS, or $dSiO_2$@MSNs were loaded at 10 mg/mL. After the loading, the particles were gently washed with PBS (5x, 1 mL). The absorbance spectra were measured with 10 mm quartz cuvettes at 0.25 mg nanoparticles/mL in PBS.

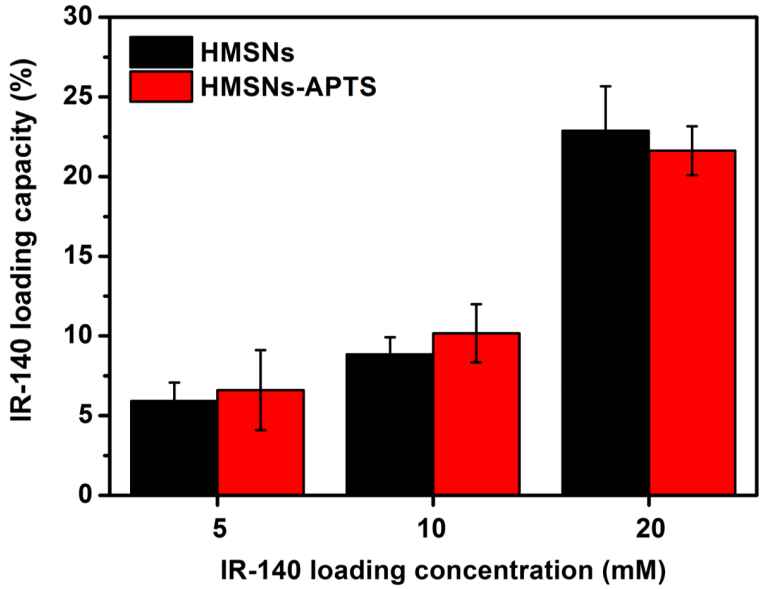

Figure S6. The loading capacity, defined as (grams IR-140/grams HMSNs or HMSNs-APTS) x 100%, of IR-140 in HMSNs (black) or HMSNs-APTS (red) at different IR-140 loading concentrations. The loading concentration of HMSNs or HMSNs-APTS was 10 mg/mL. Error represents the standard deviation of three replicates.

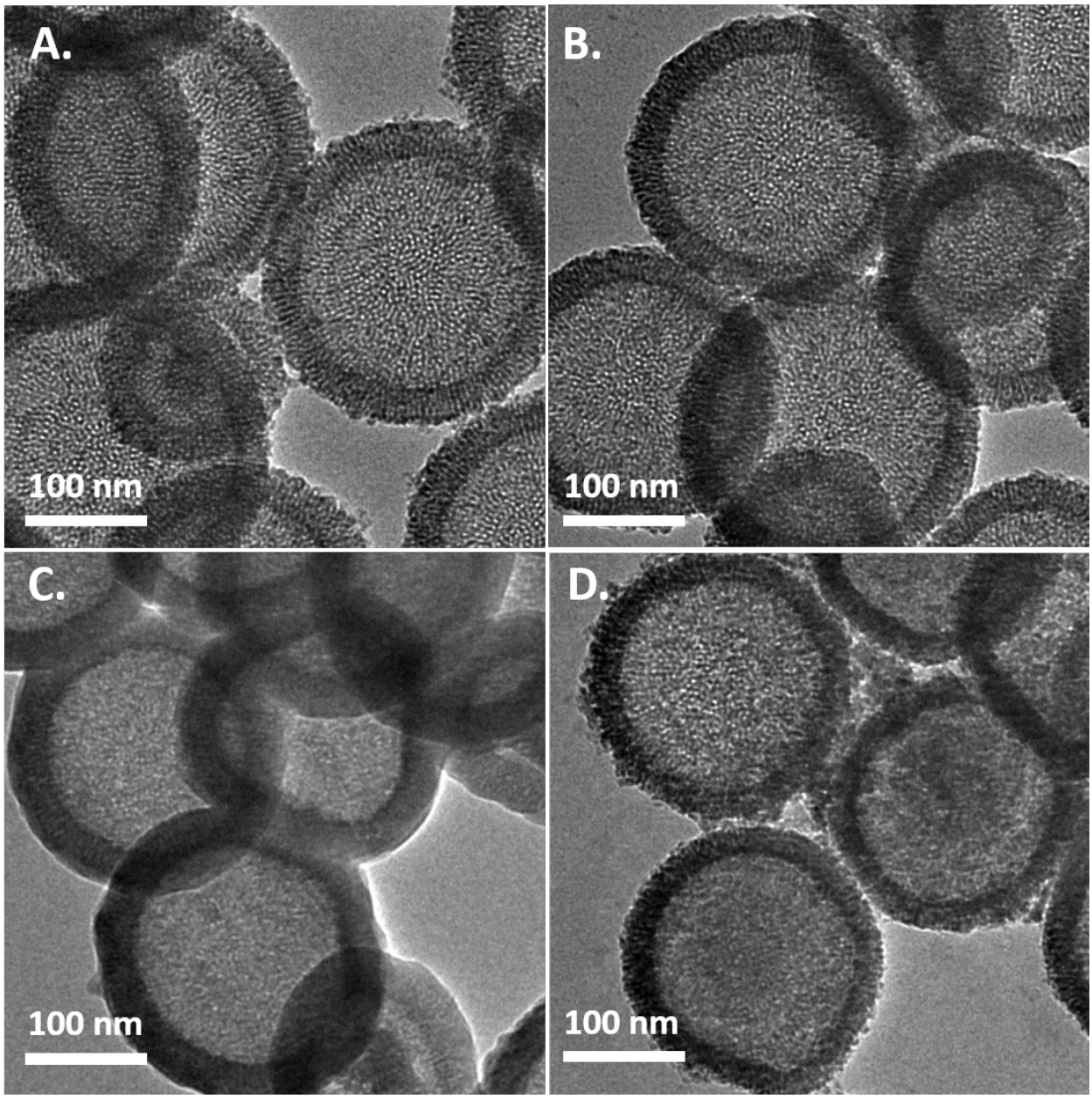

Figure S7. TEM images of HMSNs with (C) and without (A) IR-140 treatment. (A) HMSNs were dispersed in ethanol at a concentration of 0.1 mg/mL. (C) The loading concentration of IR-140 was 10 mM; HMSNs were loaded at 10 mg/mL. After loading, the particles were washed with PBS (5x, 1 mL) and dispersed in PBS at a concentration of 0.1 mg/mL. (B) As a control, HMSNs were washed with PBS (5x, 1mL) but without the loading of IR-140. After washing, HMSNs were dispersed in PBS at a concentration of 0.1 mg/mL. (D) Mixture of HMSNs with and without IR-140 treatment. The mixed particles were prepared by mixing HMSNs in PBS solution (50 μL, 0.2 mg/mL) with IR-140 loaded HMSNs in PBS solution (50 μL, 0.2 mg/mL) at the mass ratio of 1:1. TEM images were measured on a Tecnai T12 instrument with an operating voltage of 120 kV.

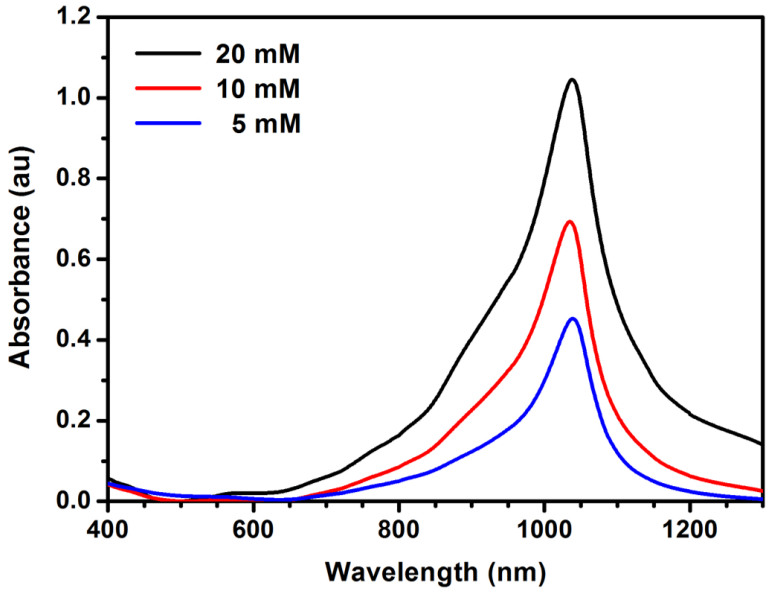

Figure S8. UV/Vis/NIR spectra of HMSNs-APTS containing IR-140 for dye loading concentrations of 20 mM (black), 10 mM (red), or 5 mM (blue) in PBS, after washing the particles with PBS (5 x 1 mL). The loading concentration of HMSNs-APTS was 10 mg/mL. The absorbance spectra were measured with 10 mm quartz cuvettes at 0.25 mg nanoparticles/mL.

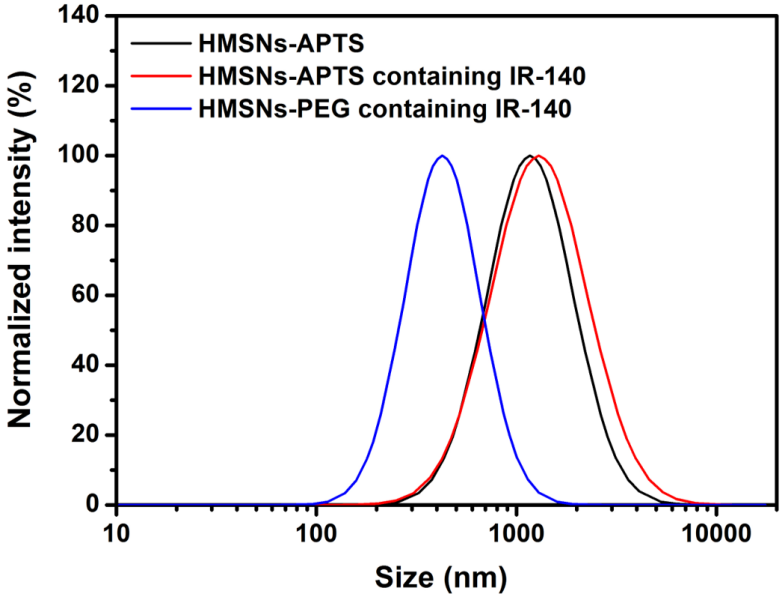

Figure S9. The dynamic light scattering size distribution of HMSNs-APTS (black), HMSNs-APTS containing IR-140 (red), and HMSNs-PEG containing IR-140 in PBS (blue) measured at 0.05 mg/mL at room temperature in PBS. Note that the HMSNs-APTS are not soluble in water and significant aggregation is observed in the DLS until after conjugation of PEG.

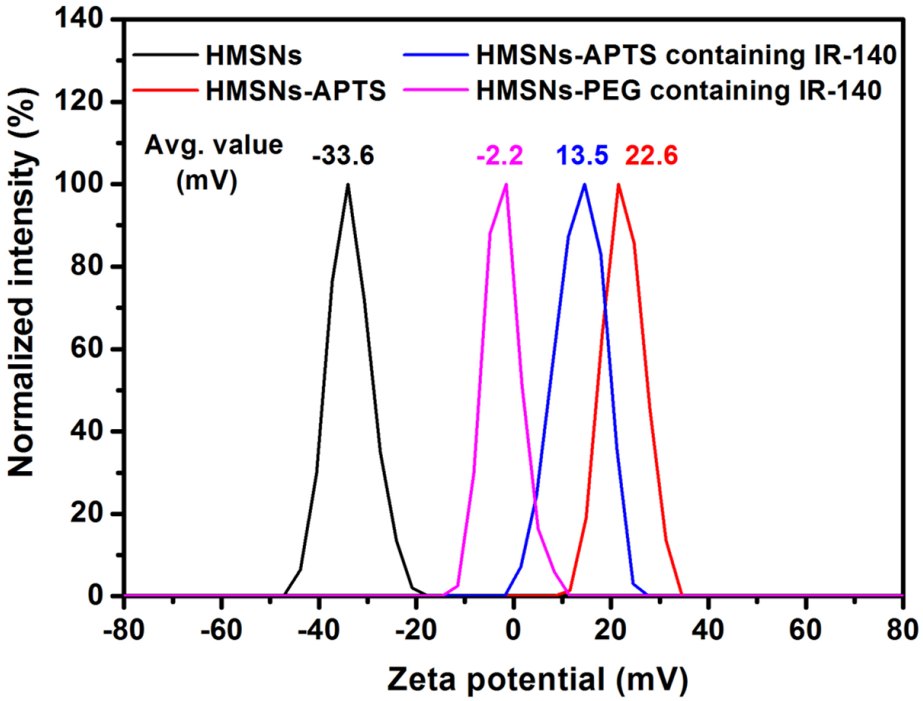

Figure S10. The zeta potential of HMSNs (black), HMSNs-APTS (red), HMSNs-APTS containing IR-140 (blue), and HMSNs-PEG containing IR-140 (pink) in D.I. water at 0.05 mg/mL at room temperature.

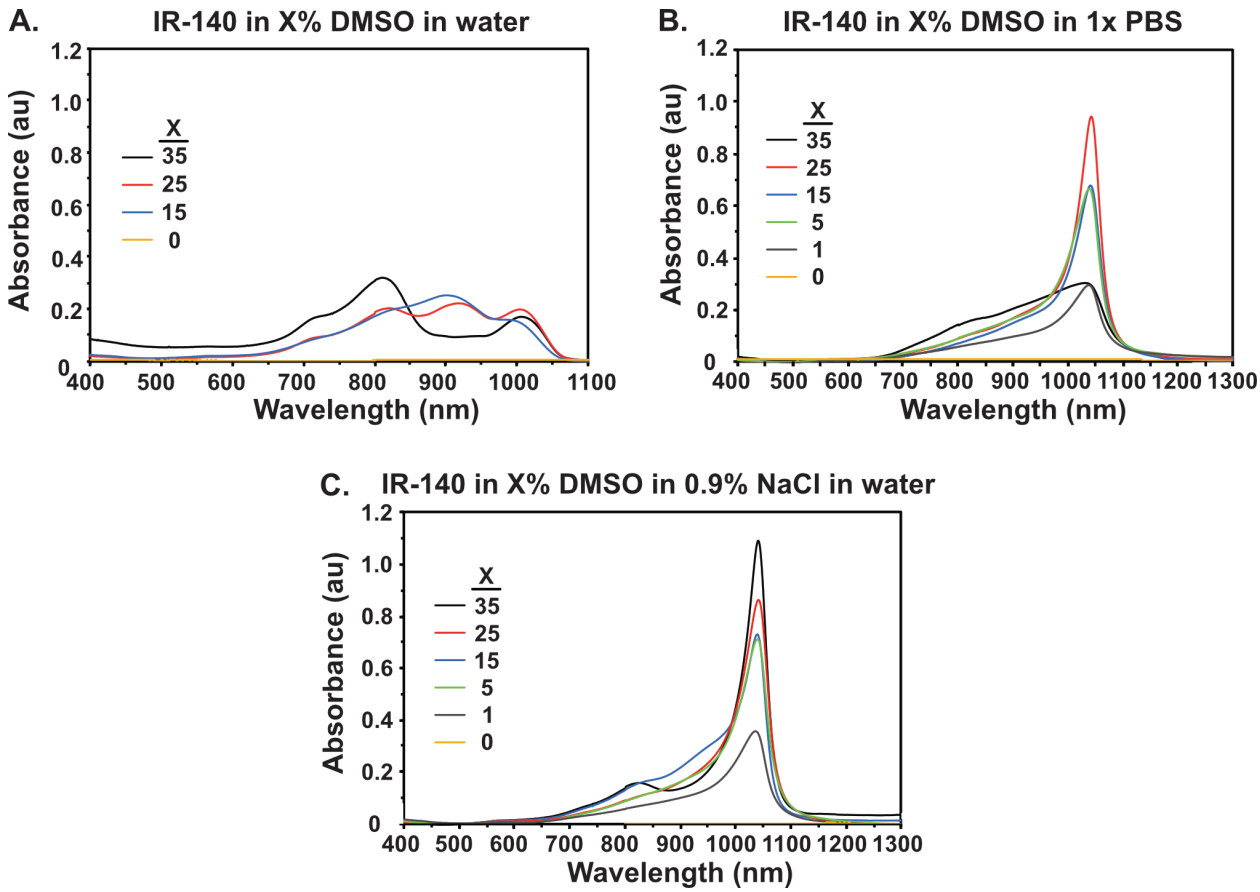

Figure S11. UV/Vis/NIR characterization of IR-140 J-aggregate formation in solution at 0.01 mg/mL in A) DMSO/water B) DMSO/1xPBS and C) DMSO/0.9% NaCl in water.

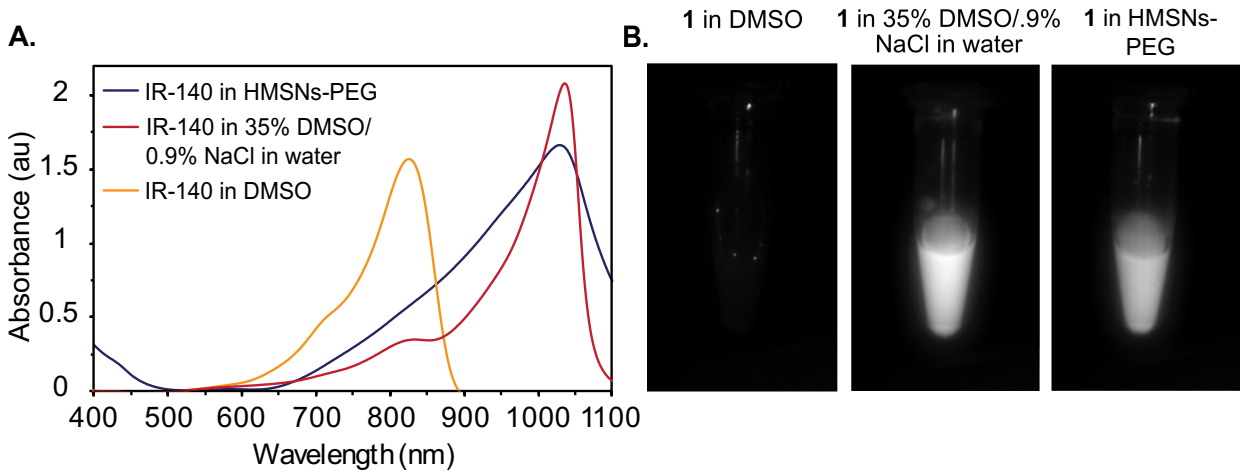

Figure S12. Emission of monomer and J-aggregate states of IR-140 under 980 nm excitation. A) Absorbance traces of samples (10 mm path length) used in vial images in B and in Figure 3B, baseline corrected to 521 nm. B) Images of IR-140 monomer in DMSO (left), IR-140 J-aggregate in solution (center) and J-aggregate in HMSNs-PEG (right) under 980 nm irradiation (99 ± 3 $mWcm^{-1}$). All Eppendorf tubes are placed in the same location, such that laser intensity across all samples is identical. See Figure 3B experimental procedure for sample preparation and acquisition settings. Displayed images were background subtracted, averaged over 10 frames and the contrast was set to identical values for comparison.

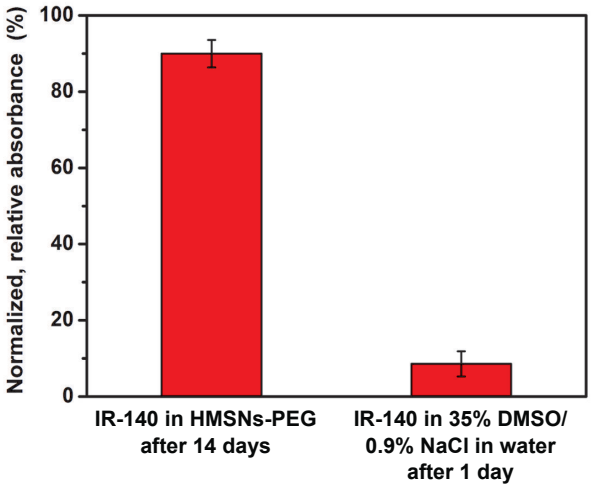

Figure S13. Stability of J-aggregates over time, displayed as the normalized, relative absorbance remaining for IR-140 in HMSNs-PEG after 14 days, and IR-140 in solution after 1 day. IR-140 loaded HMSNs-PEG were dispersed in PBS (0.25 mg/mL), and IR-140 J-aggregate was composed of 0.01 mg/mL IR-140 in 35% DMSO/0.9% NaCl in water. Error represents the standard deviation of three replicates.

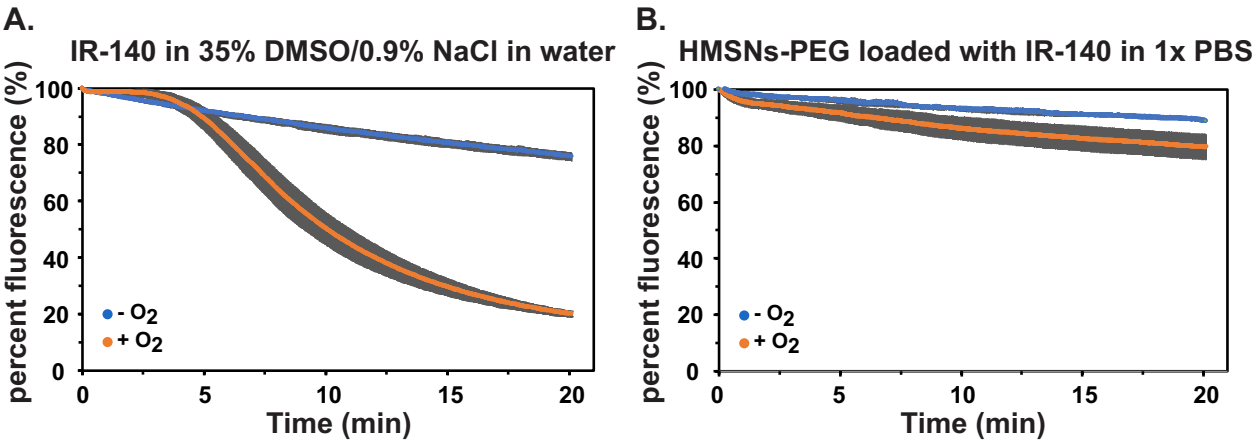

Figure S14. Photostability of J-aggregates in the presence and absence of oxygen. A) Raw data of IR-140 J-aggregate in 35 % DMSO/0.9% NaCl at 0.01 mg/mL under 980 nm irradiation with 79 $mWcm^{-2}$ power density. The relative rates of oxygenated to deoxygenated photobleaching is 7.1 to 1. B) Raw data of HMSNs-PEG loaded with IR-140 at 1.0 mg/mL in 1x PBS under 980 nm irradiation with 101 $mWcm^{-2}$ power density. The relative rates of oxygenated to deoxygenated photobleaching is 1.9 to 1. Error bars represent the standard deviation of three replicate experiments in (A) and (B) oxygenated and two replicate experiments in (B) deoxygenated. Deoxygenated samples were prepared by purging with N_2 for 30-60 min; oxygenated samples were not purged with N_2.

Note: The photobleaching rate of the solution IR-140 aggregate is substantially attenuated by the removal of oxygen, (~7x) while the photobleaching of the HMSNs IR-140 is improved by only ~2x. These data indicate that the IR-140 loaded inside the HMSNs are less affected by the presence of oxygen, which may be due to a shielding of reactive oxygen species by the dense silica shells, as suggested previously.[5]

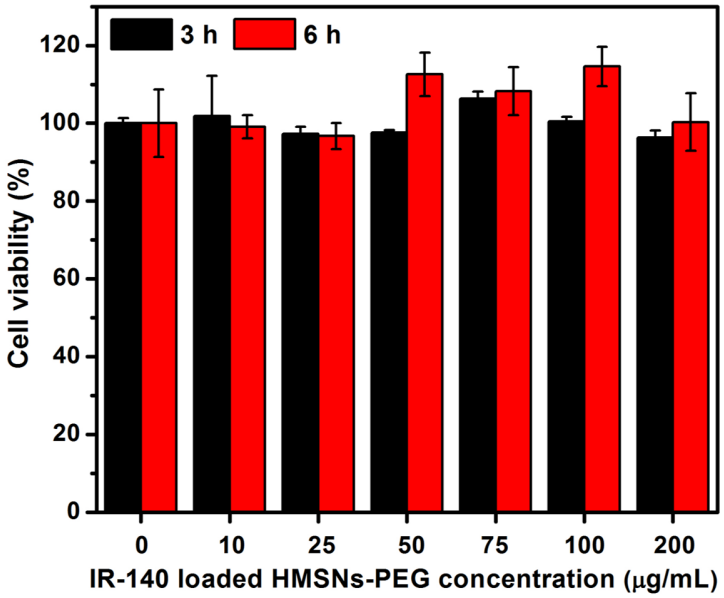

Figure S15. Cytotoxicity study of IR-140 loaded HMSNs-PEG examined by a CCK-8 assay. HeLa cells were incubated in 200 μL fresh DMEM containing 0, 2, 5, 10, 15, 20, and 40 μg of IR-140 loaded HMSNs-PEG (*i.e.* 0, 10, 25, 50, 75, 100, and 200 μg/mL) for 3 (black) or 6 (red) hours at 37 °C. The viable cells in each condition was determined by the absorbance at 450 nm and 650 nm (as a reference). The DMEM (100 μL) mixed with CCK-8 reagent (10 μL) served as a background. Error bars represent the standard deviation of three replicate experiments.

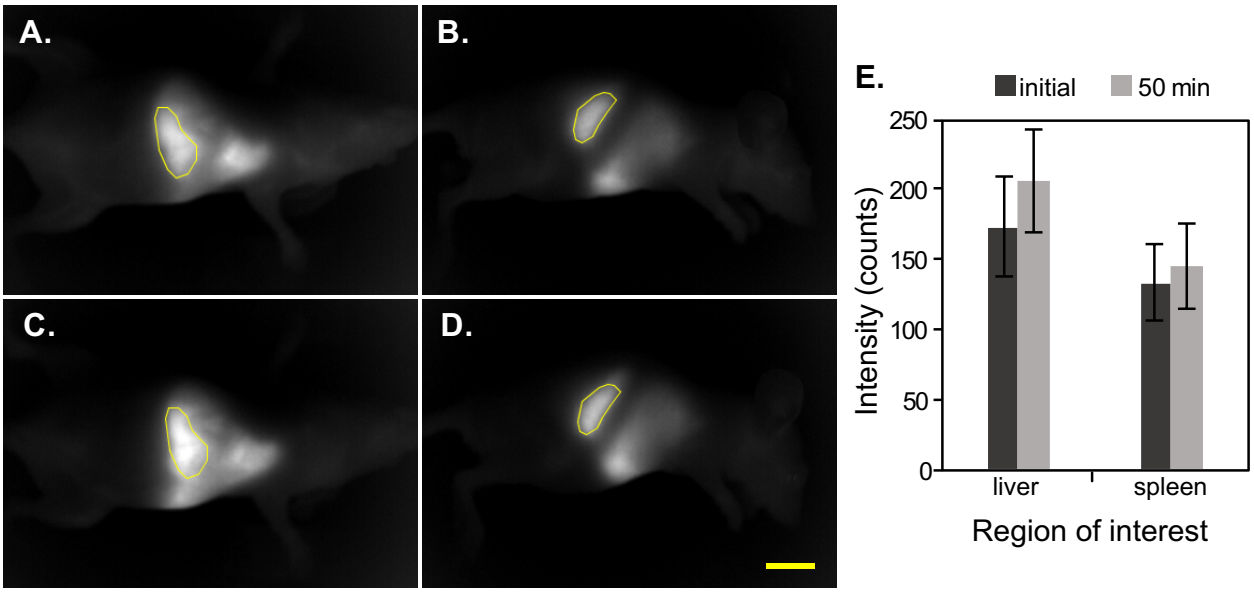

Figure S16. Images from the front (A/C) and left side (B/D) of a nude mouse directly after vascular clearance (~2 min post injection) (A/B), and after 50 min (C/D), showing uptake of IR-140 loaded HMSNs-PEG in the liver and spleen. Images were acquired with 60 ms exposure time at 16.65 fps with 980 nm ex. (91 ± 3 mW/cm^2) and 1000–1700 nm detection (see general experimental procedures (Section I) for details of optical set up). Displayed images were background subtracted, averaged over 5 frames, outliers were removed, and the contrast was set to identical values for comparison. Regions of interest were defined and applied to quantify the intensity in the liver (A/C) and spleen (B/D) over time. Scale bar represents 1 cm. E) Quantification of signal for liver and spleen showing no significant change in signal over 50 minutes. Error bars represent the standard deviation over the regions of interest. Data are representative of two replicate experiments.

V. Figure and supporting figure experimental procedures

Main text figures experimental procedures

Figure 2B
Refer to Section II "Loading of IR-140 in HMSNs, HMSNs-APTS, or $dSiO_2$@MSNs". 10 mM IR-140 was used as the loading solution. Then, IR-140 loaded HMSNs were washed by methods (a), (b), or (c) to compare the extent of IR-140 aggregate by using the above washing methods. The washing steps were repeated 5 times and finally IR-140 loaded HMSNs were re-dispersed in 1 mL of PBS solution by sonication.

Stöber silica spheres dispersed in ethanol were centrifuged (14000 rpm, 15 min) and washed with DMSO 3 times before IR-140 loading. Afterwards, Stöber silica spheres were dispersed in 200 μL of DMSO solution containing 10 mM IR-140 by sonication in a bath sonicator for 10 min. Then, the solution was stirred for 20 h. After the IR-140 loading, the solution containing the particles was centrifuged (14000 rpm, 15 min) to get IR-140 loaded Stöber silica spheres. Then, IR-140 loaded Stöber silica spheres were washed with 1 mL of PBS by gently washing with plastic transfer pipettes to remove free DMSO. After each washing step, IR-140-loaded Stöber silica spheres were centrifuged (8000 rpm, 3 min) to remove the supernatant. The washing steps were repeated 5 times and finally IR-140-loaded Stöber silica spheres were re-dispersed in PBS solution (1 mL) by sonication. The absorbance spectra of IR-140 loaded HMSNs or IR-140 loaded Stöber silica spheres were measured with 10 mm quartz cuvettes at a concentration of 0.25 mg nanoparticles/mL PBS on a Cary 5000 UV-Vis-NIR spectrophotometer at room temperature. Absorbance traces were corrected for the non-linearity between gratings.

For the prewash spectrum, after the IR-140 (10 mM) loading, the particles solution (10 mg/mL) was diluted 1:350 with DMSO for measurement. The absorbance spectrum of the prewash sample was measured with 3 mm quartz cuvettes on a JASCO V-770 UV/Vis/NIR spectrophotometer at room temperature.

Figure 2 C/D
HMSNs and IR-140 loaded HMSNs were dispersed in ethanol and D.I. water, respectively at a concentration of 0.1 mg/mL. The suspension (5 μL) of the nanoparticles was dropped onto the carbon-coated copper grid and dried at room temperature. Transmission electron microscopy was measured on a Tecnai T12 instrument with an operating voltage of 120 kV.

Figure 3A
All absorbance and emission traces were baseline corrected and normalized. Absorbance traces were acquired on a JASCO V-770 UV/Vis/NIR spectrophotometer. The slit widths used in fluorescence spectra were 5.76 mm for excitation and 11.52 mm for emission. The step size was 1.0 nm, integration time 0.1 s, and traces were acquired after an automatic detector background subtraction.

IR-140 monomer was dissolved in DMSO and diluted to an O.D. of ~ 0.7 for absorbance and less than 0.1 for fluorescence spectroscopy (ex. 785 nm) in a 1 cm path length cuvette. The monomer

absorption trace was corrected for the non-linearity between gratings before baseline subtraction and normalization.

The IR-140 J-aggregate in 35% DMSO/0.9% NaCl was prepared by dissolving 0.02 mg of IR-140 in 350 μL DMSO, vortexing briefly, adding 650 μL 0.9% aqueous NaCl, and shaking briskly. The solution becomes warm and immediately loses the blue color. Absorbance and emission traces of the J-aggregate in solution were obtained with a 2 mm path length cuvette. For the fluorescence trace, a 10 mm path length was used on the excitation side and a 2 mm path length on the emission side. A reabsorption correction was performed on the emission trace analogous to that described in Note S2.

The IR-140 loaded HMSNs-PEG were prepared as described in the synthetic procedures, section VI. The absorbance was collected without dilution in a 10 mm cuvette. The fluorescence spectrum was obtained by diluting the sample to an O.D. of less than 0.1 in a 3 mm path length square quartz cuvette, and exciting at 885 nm with a shortpass filter (Thorlabs, FES0900).

Figure 3B
Samples consisted of IR-140 monomer: 0.01 mg/mL IR-140 in DMSO (left); IR-140 J-aggregate in solution: 0.01 mg/mL IR-140 in 35% DMSO/0.9% NaCl in water (center); IR-140 HSMNs-PEG: 1 mg/mL in PBS (right). Vials were excited with 980 nm light (with Thorlabs FESH1000) with an average power density of 99 ± 3 $mWcm^{-2}$. Power densities over the three samples were not identical due to varying distance from the excitation cube. See Figure S12 for images with consistent distances from the excitation cube. Collection was from 1000–1700 nm (1000 nm LP, Edmund Optics 84-776). The custom lens system consists of a 4f configuration with a f=750.0mm lens (Thorlabs LB1247-C) and two f=200.0mm lenses (Thorlabs LB1199-C). For ergonomic reasons a 2'' protected silver-coated elliptical mirror (PFE20-P01) mounted to a kinematic mount (Thorlabs KCB2EC/M) was used. Images were acquired at 35 ms exposure time, 16.65 fps. Displayed image was background subtracted and averaged over 6 frames.

Figure 3C
Stability of IR-140 in HMSNs-PEG over time. IR-140 loaded HMSNs-PEG were dispersed in PBS at 0.25 mg/mL. The absorbance spectra were taken in a 3 mm path length cuvette immediately (day 0) and after 14 days (day 14) on a JASCO V-770 UV/Vis/NIR spectrophotometer. The absorbance was normalized, relative to spectrum (1). Results of the triplicate experiment are presented in Figure S13.

Stability of IR-140 in solution over time. IR-140 J-aggregate was prepared in DMSO as described in Figure 3A. The aggregate absorbance in a 2 mm path length cuvette was obtained immediately (day 0) and after 17 h storage in the dark (day 1) on a JASCO V-770 UV/Vis/NIR spectrophotometer. The absorbance was normalized, relative to spectrum at day 0. Results are reproduced in triplicate in Figure S13.

Figure 3D
Three solutions were prepared: (a) 1 mg/mL solution of HMSNs-PEG containing IR-140 (b) 0.01 mg/mL IR-140 in 35% DMSO/0.9% NaCl solution, and (c) 0.01 mg/mL IR-140 in DMSO. Each solution (400 μL) was irradiated with 97 ± 3 $mWcm^{-2}$ of 980 nm (a and b) and 785 nm (c) light

and their emission was monitored by a SWIR camera. Acquisition settings were 2 fps and (a) 25 ms, (b) 15 ms, and (c) 0.3 ms. Excitation and emission settings were identical to Figure 3B. Error represents the standard deviation of three measurements.

Figure 4
The IR-140 HMSNs-PEG in PBS were sonicated (Elma S15 Elmasonic) for 30 mins prior to injection and filtered through a 40 μm nylon filter. 200 μL of the IR-140 HMSNs-PEG in PBS were injected via the tail vein and immediately imaged. The excitation flux (980 nm) had an average power density of 91 ± 3 $mWcm^{-2}$ over the field of view. Images were acquired at 60 ms exposure time and 16.65 fps, in 8-bit format. Displayed images were background subtracted with an average of 10-frames from the pre-injection time points, outliers were removed, and the stills were averaged over 5 frames.

Supporting figures experimental procedures

Figure S1
Stöber silica spheres, $dSiO_2$@MSNs, or HMSNs were dispersed in ethanol at a concentration of 0.1 mg/mL. The suspension (5 μL) of the nanoparticles was dropped onto the carbon-coated copper grid and dried at room temperature. Transmission electron microscopy was measured on a Tecnai T12 instrument with an operating voltage of 120 kV.

Figure S2
Refer to Section II "Loading of IR-140 in HMSNs, HMSNs-APTS, or $dSiO_2$@MSNs". 5 or 20 mM IR-140 was used as the loading solution. Then, IR-140 loaded HMSNs were washed by methods (a), (b), or (c). In addition, IR-140 loaded $dSiO_2$@MSNs were washed by method (b). The washing steps were repeated 5 times and finally IR-140 loaded HMSNs or IR-140 loaded $dSiO_2$@MSNs were re-dispersed in 1 mL of PBS solution by sonication. The absorbance spectra of IR-140 loaded HMSNs or IR-140 loaded $dSiO_2$@MSNs were measured with 10 mm quartz cuvettes at a concentration of 0.25 mg nanoparticles/mL PBS on a Cary 5000 UV/Vis/NIR spectrophotometer at room temperature. Absorbance traces were corrected for the non-linearity between gratings.

Figure S3
Stöber silica spheres or Stöber silica spheres-APTS were prepared and described in synthetic procedures. Stöber silica spheres or Stöber silica spheres-APTS (2 mg for each) dispersed in ethanol were centrifuged (14000 rpm, 16873 g, 15 min) and washed with DMSO 3 times before IR-140 loading. Afterwards, Stöber silica spheres or Stöber silica spheres-APTS were dispersed in 200 μL of DMSO solution containing 20, 10, or 5 mM IR-140 by sonication in a bath sonicator for 10 min. Then, the solution was stirred for 20 h. After the IR-140 loading, the solution containing the particles was centrifuged (14000 rpm, 16873 g, 15 min) to get IR-140 loaded Stöber silica spheres or Stöber silica spheres-APTS. Then, IR-140 loaded Stöber silica spheres or Stöber silica spheres-APTS were washed with 1 mL of PBS by gently washing with plastic transfer pipettes to remove free DMSO and DMSO loaded in the pores. After each washing step, IR-140 loaded Stöber silica spheres or Stöber silica spheres-APTS were centrifuged (8000 rpm, 5510 g, 3 min) to remove the supernatant. The washing steps were repeated for 5 times and finally IR-140 loaded Stöber silica spheres or Stöber silica spheres-APTS were re-dispersed in PBS solution (1

mL) by sonication. The absorbance spectra of Stöber silica spheres or Stöber silica spheres-APTS were measured with 10 mm quartz cuvettes at a concentration of 0.25 mg nanoparticles/mL PBS on a Cary 5000 UV/Vis/NIR Spectrophotometer at room temperature. Absorbance traces were corrected for the non-linearity between gratings.

For zeta potential measurement, Stöber silica spheres or Stöber silica spheres-APTS were dispersed in D.I. water (2 mL) at a concentration of 50 μg/mL. The measurement was performed on a Malvern Zetasizer Nano at room temperature.

Figure S4
HMSNs (A/B), HMSNs-APTS (C/D), and $dSiO_2$@MSNs (E/F) were prepared as described in the synthetic procedures and degassed at 120 °C under vacuum for 16 h before the measurement. The surface area and pore diameter distribution of HMSNs, HMSNs-APTS, and $dSiO_2$@MSNs were determined by Brunauer-Emmett-Teller (BET) and Barrett-Joyner-Halenda (BJH) methods, respectively.

Figure S5
HMSNs, Stöber silica spheres, Stöber silica spheres-APTS, or $dSiO_2$@MSNs (2 mg for each) dispersed in ethanol were centrifuged (14000 rpm, 16873 g, 15 min) and washed with DMSO (x3) before IR-140 loading. Afterwards, HMSNs, Stöber silica spheres, Stöber silica spheres-APTS, or $dSiO_2$@MSNs were dispersed in DMSO (200 μL) solution containing 10 mM IR-140 by sonication in a bath sonicator for 10 min. Then, the solution was stirred for 20 h. After the IR-140 loading, the solution containing the particles was centrifuged (14000 rpm, 16873 *g*, 15 min) to get IR-140 loaded nanoparticles. Then, IR-140 loaded nanoparticles were washed with PBS (1 mL) by gently washing with plastic transfer pipettes to remove free DMSO and DMSO loaded in the pores. After each washing step, IR-140 loaded nanoparticles were centrifuged (8000 rpm, 5510 *g*, 3 min) to remove the supernatant. The washing steps were repeated (x 5) and finally IR-140 loaded nanoparticles were re-dispersed in PBS solution (1 mL) by sonication. The absorbance spectra of IR-140 loaded HMSNs, Stöber silica spheres, Stöber silica spheres-APTS, or $dSiO_2$@MSNs were measured with 10 mm quartz cuvettes at a concentration of 0.25 mg nanoparticles/mL PBS on a Cary 5000 UV/Vis/NIR Spectrophotometer at room temperature. Absorbance traces were corrected for the non-linearity between gratings.

Figure S6
The loading capacity of IR-140 in HMSNs or HMSNs-APTS was calculated based on the absorbance difference between the IR-140 DMSO solution before and after loading. After loading with IR-140 for 20 h, HMSNs or HMSNs-APTS were centrifuged (14000 rpm, 16873 *g*, 15 min) and the supernatant was collected for absorbance measurements. The loading capacity of IR-140 was calculated using the difference of maximum absorbance at 831 nm and the following definition of loading capacity (%): (mass of loaded IR-140/mass of particles) x 100.

Figure S7
(A) HMSNs were dispersed in ethanol at a concentration of 0.1 mg/mL. (B) The control HMSNs were subjected to washing by method (b) in the Section II "Loading of IR-140 in HMSNs, HMSNs-APTS, or $dSiO_2$@MSNs" but without the loading of IR-140. The particles were dispersed in PBS at a concentration of 0.1 mg/mL. (C) Refer to Section II "Loading of IR-140 in HMSNs,

HMSNs-APTS, or $dSiO_2$@MSNs". 10 mM IR-140 was used as the loading solution. IR-140 loaded HMSNs were dispersed in PBS at a concentration of 0.1 mg/mL. (D) The mixed samples were prepared by mixing 50 μL of HMSNs in PBS solution (0.2 mg/mL) and 50 μL of IR-140 loaded HMSNs in PBS solution (0.2 mg/mL) and were sonicated in a water bath sonicator for 20 s. The suspension (5 μL) of each of the nanoparticles was dropped onto the carbon-coated copper grid and dried at room temperature. Transmission electron microscopy was measured on a Tecnai T12 instrument with an operating voltage of 120 kV.

Figure S8

HMSNs-APTS (2 mg) dispersed in ethanol were centrifuged (14000 rpm, 16873 g, 15 min) and washed with DMSO (3 x 1 mL) before IR-140 loading. Afterwards, HMSNs-APTS was dispersed in 200 μL of DMSO solution containing 5, 10, or 20 mM IR-140 by sonication in a bath sonicator for 10 min. Then, the solution was stirred for 20 h to let IR-140 diffuse into the pores and cavity of HMSNs-APTS. After the IR-140 loading, the solution containing the particles was centrifuged (14000 rpm, 16873 g, 15 min) to get IR-140 loaded HMSNs-APTS. Then, IR-140 loaded HMSNs-APTS were washed with PBS (1 mL) by gently washing with plastic transfer pipettes to remove free DMSO and DMSO loaded in the pores. After each washing step, IR-140 loaded HMSNs-APTS were centrifuged (8000 rpm, 5510 g, 3 min) to remove the supernatant. The washing steps were repeated 5 times and finally IR-140 loaded HMSNs-APTS were re-dispersed PBS (1 mL) by sonication. The absorbance spectra of IR-140 loaded HMSNs-APTS were measured with 10 mm quartz cuvettes at a concentration of 0.25 mg nanoparticles/mL PBS on a Cary 5000 UV/Vis/NIR Spectrophotometer at room temperature. Absorbance traces were corrected for the non-linearity between gratings.

Figure S9

Refer to Section II "Loading of IR-140 in HMSNs, HMSNs-APTS, or $dSiO_2$@MSNs". 20 mM IR-140 was used as the loading solution. The loading concentration of HMSNs-APTS was 10 mg/mL. Then, IR-140 loaded HMSNs-APTS were washed by method (b). The washing steps were repeated 5 times and finally IR-140 loaded HMSNs-APTS were re-dispersed in PBS (1 mL) by sonication. The synthetic procedures of PEGylation of IR-140 loaded HMSNs-APTS can be referred to Section II "PEG conjugation on the surface of IR-140 loaded HMSNs-APTS". For dynamic light scattering size measurement, HMSNs-APTS, HMSNs-APTS containing IR-140, and HMSNs-PEG containing IR-140 were dispersed in PBS (2 mL) at a concentration of 50 μg/mL. The measurement was performed on a ZETAPALS instrument with a 660 nm red diode laser at room temperature.

Figure S10

Refer to Section II "Loading of IR-140 in HMSNs, HMSNs-APTS, or $dSiO_2$@MSNs". 20 mM IR-140 was used as the loading solution. The loading concentration of HMSNs-APTS was 10 mg/mL. Then, IR-140 loaded HMSNs-APTS were washed by method (b). The washing steps were repeated 5 times and finally IR-140 loaded HMSNs-APTS were re-dispersed in 1 mL of PBS solution by sonication. The synthetic procedures of PEGylation of IR-140 loaded HMSNs-APTS can be referred to Section II "PEG conjugation on the surface of IR-140 loaded HMSNs-APTS". For zeta potential measurement, HMSNs, HMSNs-APTS, HMSNs-APTS containing IR-140, and HMSNs-PEG containing IR-140 were dispersed in D.I. water (2 mL) at a concentration of 50 μg/mL. The measurement was performed on a Malvern Zetasizer Nano at room temperature.

Figure S11
Samples were prepared as by dissolving 0.02 mg IR-140 in DMSO, and then adding to the appropriate aqueous phase (either MilliQ water, 1x PBS, or 0.9% NaCl in water) and shaking vigorously. The appropriate volumes of DMSO and aqueous phase were used to sum to 2.0 mL for each listed percentage. For the 0% DMSO traces, IR-140 is at its solubility limit, after sonicating 0.02 mg IR-140 in 1.0 mL of the appropriate solvent for 4 hours. Absorbance traces were measured in a 3.0 mm cuvette with blanking to the appropriate solvent mixture on a JASCO V-770 UV-Vis-NIR spectrophotometer.

Figure S12
Samples were prepared and excitation and acquisition was performed as described in Figure 3B. Absorbance traces were acquired on a Shimadzu UV-1800 UV-Visible Scanning Spectrophotometer.

Figure S13
IR-140 loaded HMSNs-PEG, obtained as described in the experimental procedures II "PEG conjugation on the surface of IR-140 loaded HMSNs-APTS," were dispersed in PBS (0.25 mg/mL). The absorbance spectra were taken in a 3 mm path length cuvette immediately (day 0) and after 14 days storage in the dark. IR-140 J-aggregate in solution was prepared by dissolving 0.02 mg IR-140 in 700 μL DMSO, and subsequently adding 1.3 mL 0.9% NaCl and briskly shaking. The aggregate absorbance in a 2 mm path length cuvette was obtained immediately and after 24 h storage in the dark.

Figure S14
(A) Deoxygenated IR-140 solution J-aggregates were prepared by adding DMSO (1.4 mL) to IR-140 (0.04 mg) in a purged dram vial, followed by 0.9% NaCl solution in water (2.6 mL) and shaking. Solvents were deoxygenated by purging with N_2 for at least one hour. Oxygenated IR-140 solution J-aggregates were prepared analogously, but with solvents which had been exposed to air. Solutions (4 mL), sealed with septa, were irradiated for 20 min. The optical parameters for experiment in (A) consisted of the following: a 4-inch square first-surface silver mirror (Edmund Optics, 84448) was used to direct the emitted light through a custom filter set (Edmund optics #84-776, TL) to an Allied Vision Goldeye G-032 Cool TEC2 camera at -20 °C, equipped with a C-mount camera lens (Navitar, SWIR-35). Excitation light was passed through a positive achromat (Thorlabs AC254-050-B), 1000 nm shortpass filter (Thorlabs FESH 1100), and an engineered diffuser (Thorlabs ED1-S20-MD) to provide uniform illumination over the working area. Exposure time used was 100 ms, with 2 fps.

(B) IR-140 containing HMSNs-PEG were prepared according to experimental procedures II, sections "Loading of IR-140 in HMSNs, HMSNs-APTS, or $dSiO_2$@MSNs" and "PEG conjugation on the surface of IR-140 loaded HMSNs-APTS". Deoxygenated solutions were purged with N_2 for at least 30 min, while oxygenated were left open to air. Both sample types (1 mg/L, 0.40 mL), sealed with septa, were irradiated for 20 minutes. The optical parameters for experiment in (B) consisted of the following: a 4-inch square first-surface silver mirror (Edmund Optics, 84448) was used to direct the emitted light through a custom filter set (Edmund optics #84-776, 3x FELH1000,) to an Allied Vision Goldeye G-032 Cool TEC2 camera at -20 °C, equipped

with a C-mount camera lens (Navitar, SWIR-35). Excitation light was passed through a positive achromat (Thorlabs AC254-050-B), 1000 nm shortpass filter (Thorlabs FESH 1000), and an engineered diffuser (Thorlabs ED1-S20-MD) to provide uniform illumination over the working area. Exposure time used was 200 ms, with 2 fps.

Data were analyzed analogous to that discussed in Note S4, however only the relative rates between oxygenated and deoxygenated experiments were calculated and evaluated.

Figure S15
The viabilities of HeLa cells after the treatment of IR-140 loaded HMSNs-PEG were examined by using a cell counting kit-8 (CCK-8) assay. The cells were seeded in 96-well plates at a density of 5 x 10^3 cells per well in 200 μL DMEM supplemented with 10% FBS and 1% antibiotics in a humidity-controlled incubator at 37 °C for 24 h attachment. After the attachment, the medium was removed and the cells were incubated in 200 μL fresh DMEM containing 0, 2, 5, 10, 15, 20, and 40 μg of IR-140 loaded HMSNs-PEG (*i.e.* 0, 10, 25, 50, 75, 100, and 200 μg/mL) for 3 or 6 h in an incubator at 37 °C. After incubation, the medium was removed and the treated cells were washed with DPBS 1 time (200 μL). To measure the cell viability, 100 μL of DMEM and 10 μL of CCK-8 cellular cytotoxicity reagent were added to each well. Then, the plates were put in the incubator for 2 h at 37 °C. To measure the number of the viable cells in each condition, a plate reader (Tecan M1000) was used to measure the absorbance at 450 nm and 650 nm (as a reference). The DMEM (100 μL) mixed with CCK-8 reagent (10 μL) served as a background control.

Figure S16
Refer to Figure 4 experimental procedures.

VI. Supporting tables

Table S1. Photophysical characterization of **1**

Species	$\lambda_{max,abs}$ (nm)	ε ($M^{-1}cm^{-1}$)	$\lambda_{max,em}$ (nm)	Φ (%)
1 monomer [a]	826	$1.7 \pm 0.1 \times 10^5$	875	20[6]
1 J-aggregate [b]	1042	$3.9 \pm 0.4 \times 10^5$	1043	0.012 ± 0.007

[a] in DMSO
[b] in 35% DMSO/0.9% NaCl in water

Table S2. Photobleaching rates

Species	λ_{ex} (nm)	k_{raw} (s^{-1}) x 10^3	k_{rel} (s^{-1}) x 10^3	Relative stability
1 monomer	785	19.54 ± 0.04	19 ± 1	1
1 J-aggregate	980	1.276 ± 0.008	1.28 ± 0.05	15 ± 1
1 in HMSNs-PEG	980	0.317 ± 0.002	0.32 ± 0.01	62 ± 5

VII. Supplementary notes

Note S1: Estimation of the amount of dye molecules in a single HMSN and HMSN-PEG
In order to calculate how many IR-140 molecules loaded in a single HMSN or HMSN-APTS, we need to estimate the mass of a single HMSN or HMSN-APTS using the equation:

$$m_{amorphous\ silica} = V_{amorphous\ silica} \times \rho_{amorphous\ silica} \qquad (1)$$

Amorphous silica is defined as the silica in HMSNs shell excluding mesopores. The density (ρ) of amorphous silica is known to be 2.5 (g/cm^3 amorphous silica). There are several ways to estimate the volume of a single MSNs, as we have published previously.[7] Here, we started to determine the shell volume of a single HMSN (V_{shell}) from the equation below:

$$V_{shell} = \frac{4\pi}{3} \times \left({R_1}^3 - {R_2}^3\right) = V_{mesopore} + V_{amorphous\ silica} \qquad (2)$$

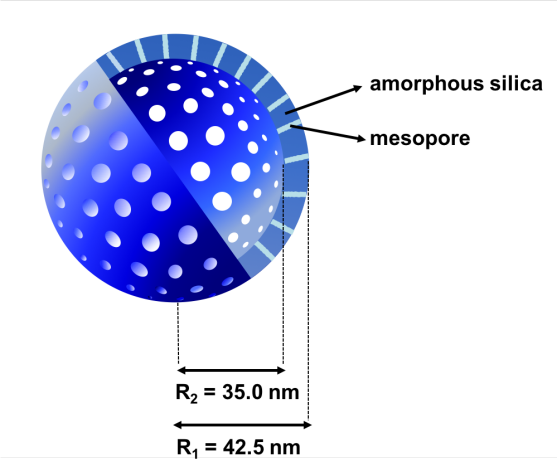

Figure S17. HMSN or HMSN-APTS used in this work. R_1 and R_2 are the outer radius and inner radius of HMSN or HMSN-APTS, respectively. V_{shell} is the shell volume of a single HMSN. $V_{mesopore}$ is the volume of the mesopores in the shell. $V_{amorphous\ silica}$ is the volume of silica in the shell excluding mesopores.

V_{shell} of the HMSNs used here (Figure S17) was calculated to be 141961 nm^3 based on equation (2). $V_{mesopore}$ was determined to be 0.94 (cm^3/g amorphous silica) from N_2 adsorption-desorption isotherm analysis.

Although we cannot directly calculate $V_{amorphous\ silica}$ from the equation (2) at this point because $V_{mesopore}$ is a function of the mass of amorphous silica, we can first determine the ratio (a) between $V_{mesopore}$ and $V_{amorphous\ silica}$ which would facilitate determination of $V_{amorphous\ silica}$.

$$V_{mesopore} \div V_{amorphous\ silica} = a \qquad (3)$$

From the density of amorphous silica, 1 g of amorphous silica has a volume of 0.4 cm^3, and thus $a = 2.35$, which is derived from $V_{mesopore}/V_{amorphous\ silica} = 0.94\ cm^3/0.4\ cm^3$. Now, plug the ratio in equation (2):

$$V_{shell} = V_{mesopore} + V_{amorphous\ silica} = 2.35\, V_{amorphous\ silica} + V_{amorphous\ silica} = 3.35\, V_{amorphous\ silica} \quad (4)$$

From above, we determine that the percentage (b) of $V_{amorphous\ silica}$ occupying V_{shell} is:

$$(V_{amorphous\ silica} \div V_{shell}) \times 100\ \% = b \quad (5)$$

b was calculated to be 30%. Since we already calculated V_{shell} to be 141961 nm^3, $V_{amorphous\ silica}$ was then determined to be 42446 nm^3 from (5). The mass of a single HMSN ($m_{amorphous\ silica}$) was then calculated by plugging in $V_{amorphous\ silica}$ in the equation (1), which was determined to be 1.06×10^{-16} (g).

To estimate the amount of dye molecules in a single HMSN, the average loading capacities of IR-140 in HMSNs (5.9 ± 1.2 %, 8.9 ± 1.1 %, and 22.9 ± 2.8 % with 5 mM, 10 mM, and 20 mM IR-140 as the loading solution, respectively) were used to determine the mass of IR-140 loaded in a single HMSN. Then, the number of IR-140 molecules loaded in a single HMSN could be calculated as:

number of IR-140 molecules loaded in a single HMSN = [(the loading capacity of IR-140 in HMSNs) $\times$ $m_{amorphous\ silica}$ $\div$ molecular weight of IR-140] $\times$ N_A (6)

where N_A is the Avogadro's constant. For example, using equation (6), with 5 mM IR-140, the number of IR-140 molecules loaded in a single HMSN was then determined to be $4.87 \times 10^3 \pm 0.99 \times 10^3$ molecules. The number of IR-140 molecules loaded in a single HMSN with 10 and 20 mM IR-140 were $7.35 \times 10^3 \pm 0.91 \times 10^3$ and $1.89 \times 10^4 \pm 0.23 \times 10^4$, respectively.

By applying the above calculation to HMSNs-APTS, we can also estimate how many IR-140 molecules were loaded in a single HMSN-APTS. Given that $V_{mesopore}$ of HMSNs-APTS is 0.73 cm^3/g, the mass of a single HMSN-APTS is calculated to be 1.26×10^{-16} g.

Given that the loading capacity of IR-140 in HMSN-APTS is 6.6 ± 2.5 %, 10.2 ± 1.8 %, and 21.6 ± 1.5 % with 5, 10, and 20 mM IR-140, respectively, the number of IR-140 molecules loaded in a single HMSN-APTS were estimated to be $6.43 \times 10^3 \pm 2.44 \times 10^3$, $9.94 \times 10^3 \pm 1.76 \times 10^3$, and $2.10 \times 10^4 \pm 0.15 \times 10^4$, respectively.

Note S2: Absorption coefficients
Absorption coefficients were calculated according to the Beer-Lambert law,

$$A = \varepsilon l c \qquad (7)$$

where A represents absorbance (unitless), ε the absorption coefficient ($M^{-1}cm^{-1}$), l the path length (cm), and c the concentration (M). Masses were determined on a microbalance and diluted using Hamilton microsyringes to concentrations within the linear range of the UV/Vis/NIR spectrophotometer. Four concentrations were obtained for each experiment and the reported error represents the standard deviation of three measurements.

The monomer absorption coefficient was straightforward as only one species is present in solution. These data were collected using a 10 mm quartz cuvette in DMSO. The raw data was corrected for non-linearity between gratings, and baseline corrected to 478 nm. The absorption coefficient at all relevant wavelengths is displayed below in Figure S18. The absorption coefficient at $\lambda_{max,abs}$ = 826 nm was 1.7 ± 0.1 x 10^5 $M^{-1}cm^{-1}$.

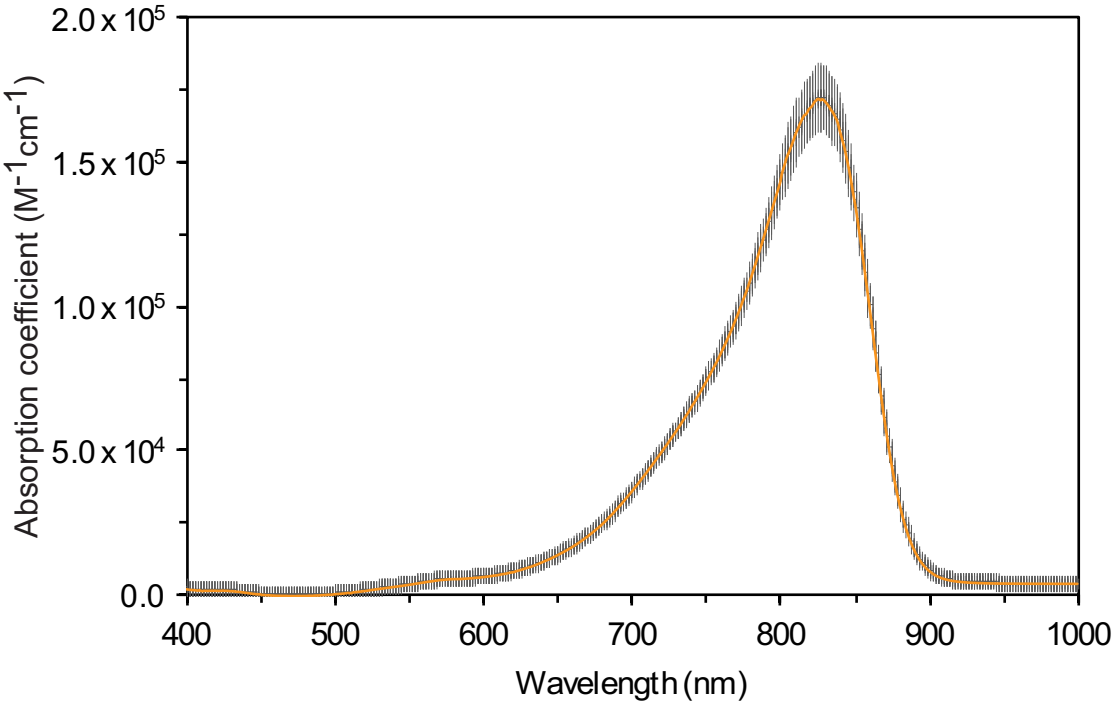

Figure S18. Absorption coefficient of IR-140 monomer in DMSO.

The J-aggregate absorption coefficient is more complex due to the requirement of high concentrations for selective formation of the J-aggregate over the monomer. As a result, to use higher concentrations, yet stay in the linear range of the spectrometer, these data were collected using a 3 mm cuvette. The raw data were baseline corrected to 449 nm and are included below in Figure S19. The uncorrected absorption coefficient (ε_{raw}) at $\lambda_{max,abs}$ = 1043 nm was 3.3 ± 0.3 x 10^5 $M^{-1}cm^{-1}$.

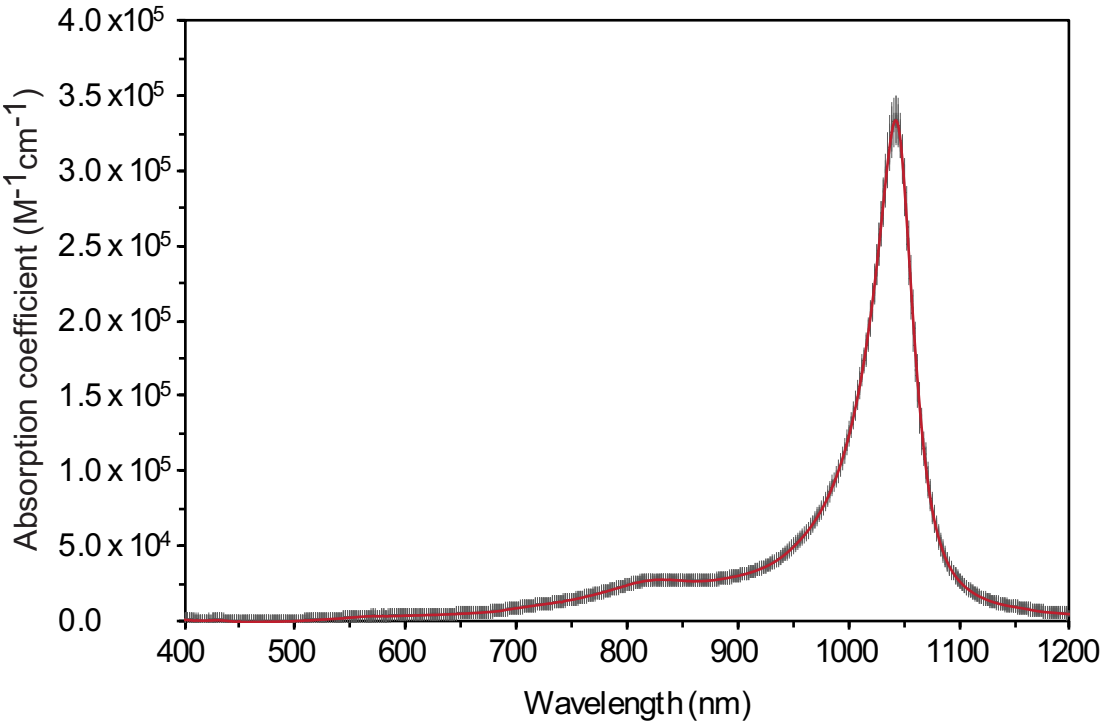

Figure S19. Uncorrected absorption coefficient of IR-140 J-aggregate in 35% DMSO/0.9% NaCl in water.

Despite the higher concentrations, some monomer remained in solution. The uncorrected data can be corrected for the remaining monomer in solution using the absorption coefficient of the monomer at its $\lambda_{max,abs}$ and making the assumption that the absorption coefficient of the monomer does not change significantly between 100% DMSO and 35% DMSO/0.9% NaCl in water. We used the equation:

$$\alpha_m + a_j = 1 \qquad (8)$$

where α_m represents the mole fraction of monomer and α_j the mole fraction of J-aggregate. The value α_m for each absorbance trace was obtained using the Beer-Lambert law from the absorption coefficient of the monomer and the known concentration of total dye. The value a_j was then used as a multiplicative factor to correct the concentration of J-aggregate in solution. The absorption coefficient was then recalculated with the corrected concentration values. The corrected absorption coefficient at $\lambda_{max,abs}$ = 1043 nm was 3.9 ± 0.4 x 10^5 $M^{-1}cm^{-1}$. Error was taken as the standard deviation of the three replicates. The corrected absorption coefficient is displayed below in Figure S20.

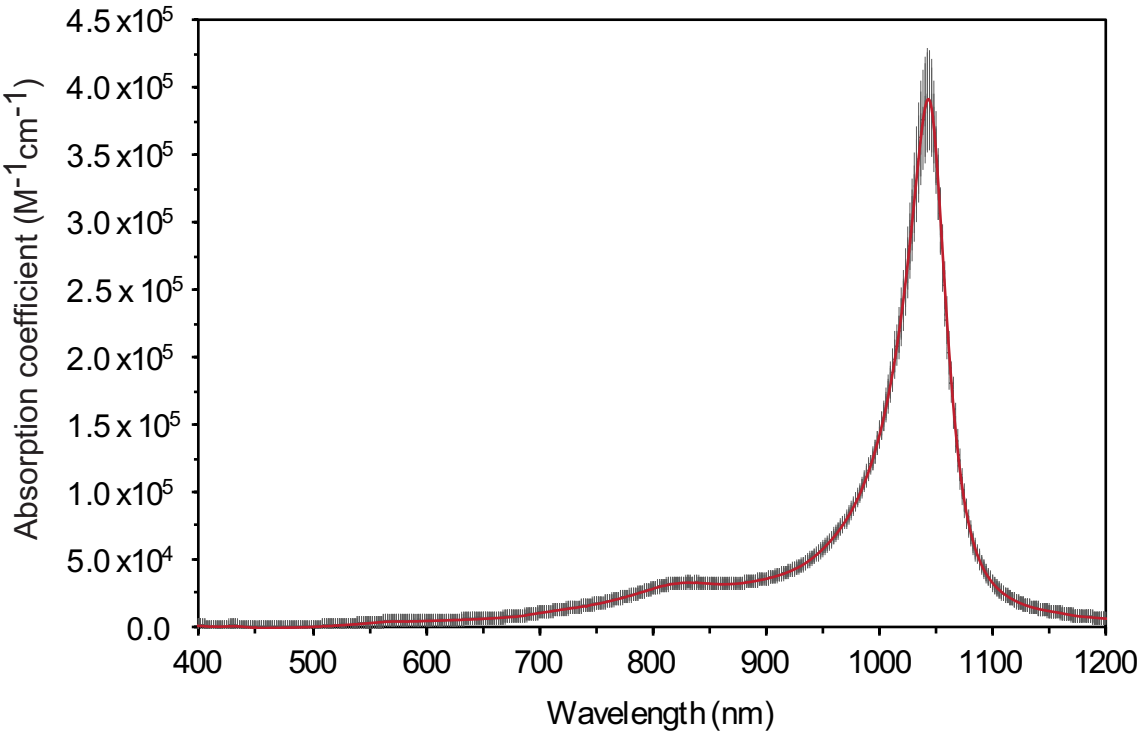

Figure S20. Corrected absorption coefficient of IR-140 J-aggregate in 35% DMSO/0.9% NaCl in water.

Note S3: Quantum yield

The photoluminescence quantum yield (Φ_F) of a molecule or material is defined as follows,

$$\Phi_F = \frac{P_E}{P_A} \qquad (9)$$

where P_E and P_A are the number of photons absorbed and emitted, respectively. To determine the quantum yield, we either use a relative method with a known standard in the same region of the electromagnetic spectrum, or an absolute method, in which the number of photons absorbed and emitted are measured independently. Here, due to the limits of our petite integrating sphere (Horiba KSPHERE-Petite with InGaAs detector Horiba Edison DSS IGA 020L), we use a relative method, with IR-26 as the known standard.

The quantum yield was measured at three different excitation wavelengths, 885 nm, 900 nm, and 915 nm and the results were averaged to obtain the value reported.

To compare an unknown to a reference with a known quantum yield, the following relationship was used:

$$\Phi_{F,x} = \Phi_{F,r}(m_x/m_f)(\eta_x{}^2/\eta_r{}^2) \qquad (10)$$

Where m represents the slope of the line (y = mx + b) obtained from graphing integrated fluorescence intensity versus optical density across a series of samples, η is the refractive index of the solvent, and the subscripts x and r represent values of the unknown and reference, respectively.

The ($\Phi_{F,r}$) of IR-26 was taken to be 0.05 ± 0.03%, as we have previously measured[8], and which agrees with several recent measurements.[6,9]

To obtain a plot of integrated fluorescence intensity versus absorbance for the reference and unknown, five solutions and a solvent blank were prepared and their absorbance and emission spectra were acquired. IR-26 was diluted in DCE to concentrations with optical densities less than 0.1 to minimize effects of reabsorption. The baseline corrected (to 1500 nm) fluorescence traces were integrated from 950 – 1500 nm, and the raw integrals were corrected by subtracting the integral over an identical range from fluorescence traces of the blank solvent (Figure S21A). The methods employed here were validated with comparison of IR-26 to IR-1061, giving a Φ_F value of 0.3 ± 0.2 %, which is in agreement with our prior absolute quantum yield measurement,[8] but with lower precision due to the uncertainty in IR-26 absolute Φ_F.

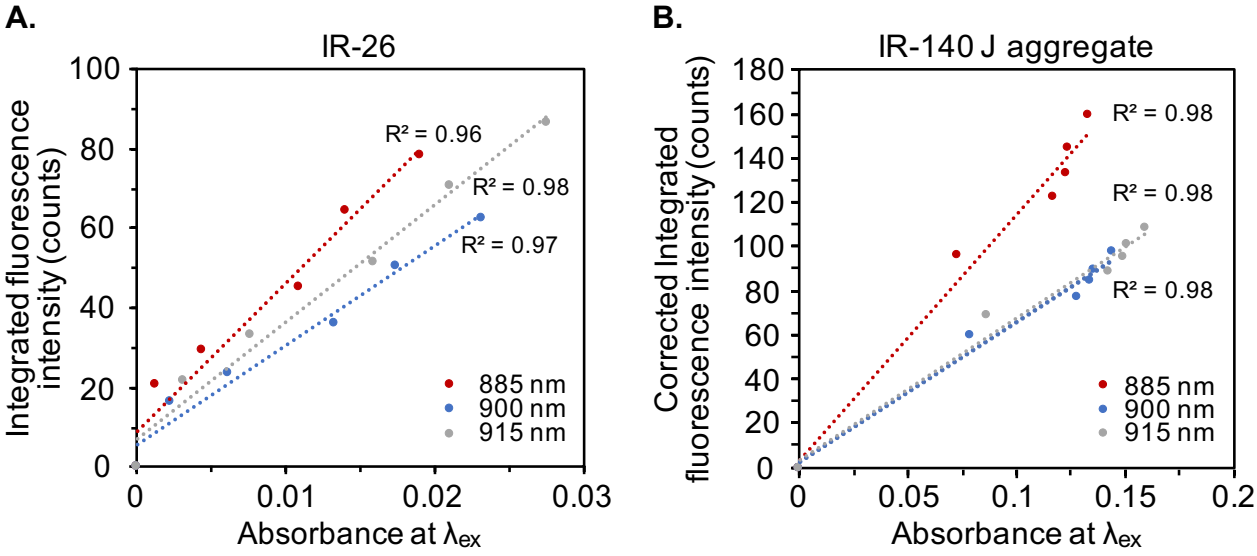

Figure S21. Solvent corrected integrated fluorescence intensity versus absorbance plots for A) IR-26 and B) IR-140 J-aggregate, also corrected for reabsorption.

The IR-140 J-aggregate was prepared as described in Figure 3A, in 35% DMSO/0.9% NaCl in water. Due to the necessity of using concentrated samples for IR-140 to remain in the J2 aggregate state, high concentrations of IR-140 J-aggregate were used for quantum yield measurements (the OD with a 2 mm path length at the relevant excitation wavelengths ranged from 0.07 – 0.16). The baseline corrected (to 1400 nm) fluorescence traces of the optically dense IR-140 J-aggregate samples were corrected for reabsorption by the relationship,

$$I(\lambda) = I_o(\lambda)[-\ln(10^{-OD(\lambda)})/(1-10^{-OD(\lambda)})] \qquad (11)$$

where $I(\lambda)$ and $I_o(\lambda)$ are the corrected and experimental fluorescence intensities at each

wavelength, and $OD(\lambda)$ is the optical density of the sample at the corresponding wavelength. The corrected fluorescence traces were then integrated from 965 nm – 1400 nm, and the raw integrals were corrected by subtracting the integral over an identical range from fluorescence traces of the blank solvent.

The integrated fluorescence intensities were then plotted against the baseline corrected absorbance values at the relevant wavelength, and the slope and error in slope were obtained ($R^2 > 0.95$ for all traces) (Figure S21B)

The refractive index for DCE was taken as 1.440[10], while that of the 35% DMSO/0.9% NaCl solution in water was approximated as a binary mixture of 35% DMSO in water and taken to be 1.383.[11] Both values were designated to have a precision to ± 0.001.

The average quantum yield value (over 885 nm, 900 nm, and 915 nm excitations) was calculated to be 0.012 ± 0.007. Errors were propagated from the error in IR-26 Φ_F (± 0.03)[8], slope of the integrated fluorescence intensity versus optical density plot (unique for each trace, but ranged from 7-10% of the slope value), and refractive indices (± 0.001).

For quantum yield measurements, fluorescence traces were acquired with ex. 885 nm, 900 nm, and 915 nm with a 950 nm shortpass filter (Thorlabs FESH0950) and collection from 950–1400 nm for IR-140 J-aggregate and 950–1500 for IR-26. The slits were 5.76 mm for excitation and 11.52 mm for emission. The step size used was 1.0 nm, integration time 0.1 s, and traces were acquired after an automatic detector background subtraction, and with the default excitation correction. All absorbance and fluorescence traces were taken in a 10 mm x 2 mm path length cuvette. For absorbance traces, the 2 mm path length was used, while emission traces were acquired with 10 mm at the excitation side and 2 mm on the emission side, with emission detection occurring at 90° from excitation.

Note S4: Photobleaching rates

All photobleaching data were fit to a mono-exponential decay and the rate constants were obtained from the first order reaction equation:

$$\ln[A] = -kt + \ln[A]_o \qquad (12)$$

where A and A_o represent the emission collected at time t and the initial emission collected, respectively. All R^2 values were > 0.96. Error bars represent the standard deviation of three measurements. If a change in slope occurred in the ln[A] values (*i.e.* in the IR-140 J-aggregate bleaching in 35% DMSO/0.9% NaCl in water solution), the rate was taken as the initial rate and the lines were fit only to the linear region (Figure S22). This analysis conservatively estimates the photobleaching rate of the solution phase aggregate as slower than it appeared in subsequent time points (see Figure 3D).

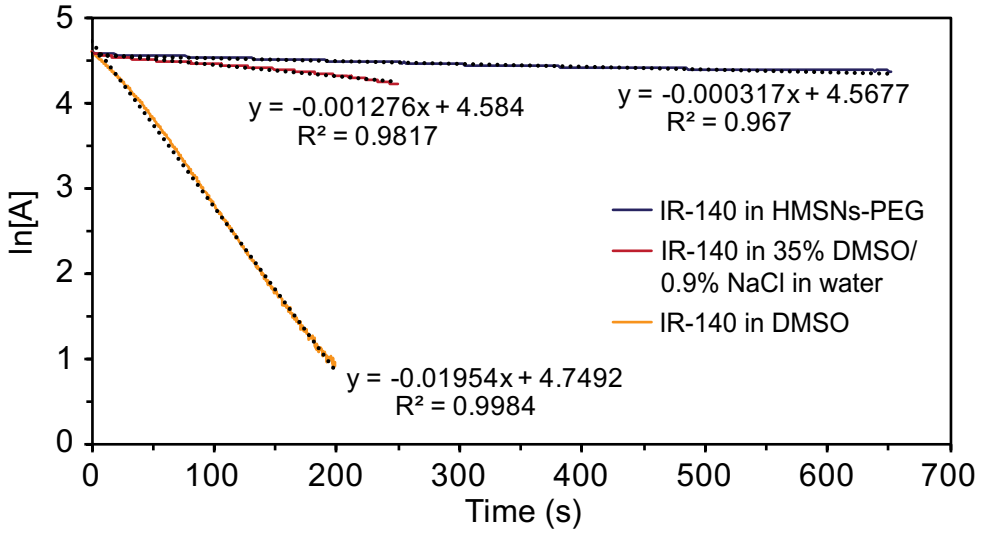

Figure S22. Photobleaching data plotted as the ln[A] vs time and the corresponding linear fits.

To compare photobleaching rates between samples irradiated at distinct wavelengths, it is necessary to consider the relative number of photons absorbed by each species. This requires corrections for (1) the difference in photon energy between the two wavelengths, and (2) the difference in photons absorbed by the two samples.

To account for photons of different energy, we go back to the common unit of number of photons per second per surface unit *Np,* ($cm^{-2}s^{-1}$). This value can be obtained by first calculating energy of a photon *Ep,* (J) at the wavelength of irradiation:

$$E_p = \frac{hc}{\lambda} \qquad (13)$$

where *h* is Planck's constant, and *c* the speed of light. The *Np* can then be found from the irradiance *I* (Wcm^{-2}) and *Ep* by the following equation:

$$N_p = \frac{I}{E_p} \qquad (14)$$

The *Np* for 980 nm and 785 nm light is 4.8 x 10^{17} and 3.8 x 10^{17} $cm^{-2}s^{-1}$, respectively.

To account for the difference in photons absorbed, we use the absorption coefficients at the wavelength of irradiation, λ_{ex}. For the IR-140 J-aggregate, the corrected absorption value was used. The absorption coefficient of IR-140 in HMSNs-PEG was taken to be that of the J-aggregate in solution. The relative values of $N_p \times \varepsilon$ can then be compared to obtain a ratio, *X* for each wavelength,

$$X_{785} = (N_{p,785} \times \varepsilon_m)/(N_{p,980} \times \varepsilon_j) \qquad (15)$$

$$X_{980} = (N_{p,980} \times \varepsilon_j)/(N_{p,980} \times \varepsilon_j) \qquad (16)$$

where ε_m and ε_j represent the aborbance coefficient of the monomer and J-aggregate, respectively, at their appropriate excitation wavelength, λ_{ex}. The ratio X_{785} was calculated to be 0.998, providing a correction factor for the relative number of photons absorbed per second in the

785 nm experiment compared to the 980 nm experiments, while the ratio X_{980} is 1.000. These values can be related to the relative rate, k_{rel} by the equation:

$$k_{rel} = \frac{k_{raw}}{X} \qquad (17)$$

The relative rates with intermediate values used in the calculations are listed below in Table S3.

Table S3. Photobleaching rates and values used in calculations and corrections.

Sample	λ_{ex} (nm)	Fluence ($mWcm^{-2}$)	k_{raw} (s^{-1}) x 10^3	ε at λ_i ($M^{-1}cm^{-1}$) x 10^{-5}	N_p	k_{rel} (s^{-1}) x 10^3	Relative stability
1 monomer	785	97 ± 3	19.54 ± .04	1.18 ± 0.07	3.83 x10^{17}	19 ± 1	1
1 J-aggregate	980	97 ± 3	1.276 ± 0.008	0.95 ± 0.04	4.79 x 10^{17}	1.28 ± 0.05	15 ± 1
1 in HMSNs-PEG	980	97 ± 3	0.317 ± 0.002	0.95 ± 0.04	4.79 x 10^{17}	0.32 ± 0.01	62 ± 5

VIII. References

[1] Chen, F.; Hong, H.; Shi, S.; Goel, S.; Valdovinos, H.F.; Hernandex, R.; Theuer, C.P.; Barnhart, T.E.; Cai, W. *Sci. Rep.* **2014**, *4*, 5080.

[2] Chen, W.; Tsai P.H.; Hung, Y.; Chiou, S.H.; Mou, C.Y. *ACS Nano* **2013**, *7*, 8423−8440.

[3] Zhang, Y.; Ang, C.Y.; Li, M.; Tan, S.Y.; Qu, Q.; Luo, Z.; Zhao, Y. *ACS Appl. Mater. Interfaces* **2015**, *7*, 18179-18187.

[4] Chen, W.; Cheng, C.A.; Zink, J.I. "Spatial, Temporal, and Dose Control of Drug Delivery using Noninvasive Magnetic Stimulation." *ACS Nano* **2019**, 13, 1292-1308.

[5] Qiao, Y.; Polzer, F.; Kirmse, H.; Kirstein, S.; Rabe, J.P. "Nanohybrids from nanotubular J-aggregates and transparent silica nanoshells." *Chem. Commun.* **2015**, *51*, 11980–11982.

[6] Hatami, S.; Würth, C.; Kaiser, M.; Leubner, S.; Gabriel, S.; Bahrig, L.; Lesnyak, V.; Pauli, J.; Gaponik, N.; Eychmüller, A.; Resch-Genger, U. *Nanoscale* **2015**, *7*, 133–143.

[7] Xue, M.; Zink, J.I. *J. Phys. Chem. Lett.* **2014**, *5*, 839–842.

[8] Cosco, E. D.; Caram, J. R.; Bruns, O. T.; Franke, D.; Day, R. A.; Farr, E. P.; Bawendi, M. G.; Sletten, E. M. *Angew. Chem. Int. Ed.* **2017**, *56*, 13126–13129.

[9] Semonin, O. E.; Johnson, J. C.; Luther, J. M.; Midgett, A. G.; Nozik, A. J.; Beard, M. C. *J. Phys. Chem. Lett.* **2010**, *1*, 2445–2450.

[10] Ali, A.; Tariq, M. *Chem. Eng. Commun.* **2008**, *195*, 43–56.

[11] LeBel, R. G.; Goring, D. A. I. *J. Chem. Eng. Data* **1962**, *7*, 100–101.